

CZECH TECHNICAL UNIVERSITY IN PRAGUE  
Faculty of Electrical Engineering  
Department of Electrical Power Engineering



**Determination of Induction Motor Speed using  
Kalman Filter**

*by*

*RANJAN TIWARI*

Supervisor

Ing. PAVEL KARLOVSKY

A master thesis submitted to  
The Faculty of Electrical Engineering, Czech Technical University in  
Prague

Master Degree study program: Electrical Power Engineering  
Prague, June 2019

## I. Personal and study details

Student's name: **Tiwari Ranjan** Personal ID number: **472705**  
Faculty / Institute: **Faculty of Electrical Engineering**  
Department / Institute: **Department of Electrical Power Engineering**  
Study program: **Electrical Engineering, Power Engineering and Management**  
Branch of study: **Electrical Power Engineering**

## II. Master's thesis details

Master's thesis title in English:

**Determination of Induction Motor Speed using Kalman Filter**

Master's thesis title in Czech:

**Determination of Induction Motor Speed using Kalman Filter**

Guidelines:

- 1) Carry out a mathematical description of the Kalman filter.
- 2) Design the Kalman filter for induction motor speed determination.
- 3) Implement the designed Kalman filter on a mathematical model of induction motor using Matlab Simulink.
- 4) Implement and verify the Kalman filter on a laboratory motor using dSPACE.

Bibliography / sources:

- [1] M. S. Grewal and A. P. Andrews, Kalman Filtering Theory and Practice Using MATLAB
- [2] P. Vas, Sensorless Vector and Direct Torque Control
- [3] dSPACE DS1103 manual

Name and workplace of master's thesis supervisor:

**Ing. Pavel Karlovský, Department of Electric Drives and Traction, FEE**

Name and workplace of second master's thesis supervisor or consultant:

Date of master's thesis assignment: **18.02.2019** Deadline for master's thesis submission: **31.05.2019**

Assignment valid until: **20.09.2020**

\_\_\_\_\_  
Ing. Pavel Karlovský  
Supervisor's signature

\_\_\_\_\_  
Head of department's signature

\_\_\_\_\_  
prof. Ing. Pavel Ripka, CSc.  
Dean's signature

## III. Assignment receipt

The student acknowledges that the master's thesis is an individual work. The student must produce his thesis without the assistance of others, with the exception of provided consultations. Within the master's thesis, the author must state the names of consultants and include a list of references.

\_\_\_\_\_  
Date of assignment receipt

\_\_\_\_\_  
Student's signature

---

## *Declaration*

I, Ranjan Tiwari declare that the submitted work I have produced independently and have listed all used information sources in accordance with the Methodological Guideline on Ethical Principles of the Preparation of University Graduate Thesis.

Date:

Signature:

---

# *Abstract*

This thesis describes the design and implementation of the discretized Extended Kalman Filter (EKF) for the estimation of the speed of the induction motor. In this implementation, the speed is treated as an additional state of the system and the EKF is designed to estimate this state. The inputs for the filter are the inverter voltage and stator currents. The simulations are carried out in Matlab Simulink and after the verification of the filter, the algorithm is tested with laboratory motor. The filter is implemented on the dSPACE DS1103 microprocessor controlling unit, which also handles the real-time data logging and visualization, and the control user interface. Predictive Torque Control (PTC) strategy is employed for the motor drive. The experimental part presents the speed determination accuracy in various working points including high and low speed areas. Then the optimization of the filtering process for better response in transients and stable states are performed. Finally, the results are evaluated.

**Keywords:** Induction Motor, Extended Kalman Filter, MATLAB/Simulink, dSPACE, Sensorless Speed Determination

---

# *Abstrakt*

Tato práce popisuje návrh a implementaci diskretizovaného rozšířeného Kalmanova filtru (EKF) pro odhad rychlosti asynchronního motoru. V této implementaci EKF je rychlost motoru považována za další stav systému a filtr je navržen tak, aby odhadoval právě tento stav. Vstupem pro filtr jsou napětí na výstupu měniče a statorové proudy. Simulace jsou provedeny v prostředí Matlab Simulink a po ověření funkčnosti je algoritmus otestován i na laboratorním motoru. Filtr je realizován na mikroprocesorové řídicí jednotce dSPACE DS1103, která také obsluhuje záznam a vizualizaci dat v reálném čase a uživatelské rozhraní ovládání. Pro řízení pohonu je použita strategie prediktivního řízení momentu (PTC). V experimentální části je předvedena přesnost stanovení rychlosti v různých pracovních bodech včetně oblastí vysokých a nízkých otáček. Dále je provedena optimalizace filtru pro lepší odezvu v přechodových dějích i ve stabilních stavech. Nakonec je proveden rozbor získaných výsledků.

**Klíčová slova:** Asynchronní motor, Rozšířený Kalmanův filtr, MATLAB/Simulink, dSPACE, bezsenzorové zjišťování otáček

---

# *Acknowledgement*

Throughout the writing of this thesis, I have received a great deal of support and assistance. I would first like to thank my supervisor, *Ing. Pavel Karlovsky*, whose expertise was invaluable in the formulation of the project topic and methodology in particular. He was there to guide me at every step needed.

I would like to thank *Prof. Ing. Jiří Lettl, CSc*, for his assistance and guiding me towards the topic for this thesis in the initial phase. I would like to acknowledge my colleague from my class, *Emre Sakar* for his wonderful assistance during different phases of writing this thesis.

I would also like to thank the Department of Electric Drives and Traction, CTU and the faculty from there for assisting me in the laboratory issues during the experimentation phase, and letting me conduct the experimental research in the laboratory.

In addition, I would like to thank my parents for their wise counsel and sympathetic ear. Finally, there are my friends, Anup, Bishal, Dipesh, Sarjan, Madhu, Nishant, Biswash and Aastha who were there to support me and providing happy distraction to rest of my mind outside my research.



## **Dedication**

*To My Family and Friends*

---

# *Contents*

<b>LIST OF FIGURES</b>		xi
<b>ABBREVIATIONS</b>		xiii
<b>1</b>	<b>INTRODUCTION</b>	<b>1</b>
<b>2</b>	<b>KALMAN FILTER AND ITS DESIGN FOR INDUCTION MOTOR SPEED DETERMINATION</b>	<b>3</b>
2.1	Kalman Filter	3
2.1.1	The Process to be Estimated	4
2.1.2	The Estimation Process	4
2.1.3	Mathematical Representation	5
2.2	Extended Kalman Filter	5
2.2.1	Mathematical Representation	6
2.3	Mathematical Model of the Induction Motor	6
2.4	Designing and Implementing the EKF to the Motor Model	7
2.4.1	Extension of the State Vector to Add Rotor Angular Speed as a State Variable	8
2.4.2	Discretization of the IM model	9
2.4.3	Determination of the Noise and State Covariance Matrices	10
2.4.4	Implementation of EKF Algorithm	10
2.4.4.1	Initialization of State Vectors and Covariance Matrices	11
2.4.4.2	Prediction of state variables	11
2.4.4.3	Estimation of Covariance Matrix of Prediction	12
2.4.4.4	Kalman Gain Computation	12
2.4.4.5	State Vector Estimation	13
2.4.4.6	Correction of the Covariance Matrix of Prediction for next loop	13



---

<b>3</b>	<b>SIMULATION OF IM AND EKF IN SIMULINK MATLAB</b>	14
3.1	Model of IM and Control Strategy	14
3.1.1	Reference Values Block	15
3.1.2	Predictive Control Block	15
3.1.3	Inverter Block	16
3.1.4	IM Model Block	17
3.2	EKF Model	18
3.2.1	EKF Algorithm	18
3.2.2	Tuning of the Noise Covariance Matrices Q and R	20
3.3	Simulation Results from Matlab Simulink	21
3.4	Concluding the Simulation Results	27
<b>4</b>	<b>DESCRIPTION OF THE WORKPLACE AND HARDWARE ASSEMBLED</b>	28
4.1	The Circuit Diagram	28
4.2	List of Hardware Assembled	28
<b>5</b>	<b>EXPERIMENTAL RESULTS</b>	33
5.1	Steady State Operation of Motor	
5.1.1	Loaded Steady State Operation of the Motor	33
5.1.2	Unloaded steady state Operation of the Motor	34
5.1.3	Comparison of Loaded and Unloaded Operation Mode	36
5.2	Tuning of Covariance Noise Matrices Q and R	36
5.2.1	Keeping R constant and varying Q in steady state	37
5.2.2	Keeping Q constant and varying R	37
5.2.3	Varying Q while keeping R constant at 2000 in transients	38
5.3	Operations in Speed Reversal Mode with changing slew rates	40
5.4	Low Speed Performance	42
5.5	Performance under varying load	42

---

<b>6</b>	<b>CONCLUSION</b>	44
	Work for Future	45
<b>7</b>	<b>REFERENCES</b>	47
	<b>APPENDIX</b>	48
	A.1 Parameters of IM	48
	A.2 Equations of IM	48

---

# *List of Figures*

2.1	<i>Typical application of Kalman Filter</i>	3
2.2	<i>Structure of EKF</i>	11
3.1	<i>Simulink Model of the estimation of rotor speed of IM with control mechanism</i>	14
3.2	<i>Reference Values Block</i>	15
3.3	<i>Block diagram schematic of IM drive Model Predictive Control</i>	16
3.4	<i>Voltage vector diagram</i>	17
3.5	<i>IM block representation</i>	17
3.6	<i>EKF block</i>	18
3.7	<i>Simulation Results of IM parameters</i>	22
3.8	<i>Comparison of IM measured Current and EKF estimated Current</i>	22
3.9	<i>Comparison of IM measured Rotor Flux and EKF estimated Rotor Flux</i>	23
3.10	<i>Simulation comparison between Measured IM speed and EKF estimated speed for 20 <math>\mu</math>s sampling time with noise</i>	23
3.11	<i>Detailed view of the speed comparison in steady state for Figure 3.10</i>	24
3.12	<i>Simulation result comparison between Measured IM speed and EKF estimated speed for 150<math>\mu</math>s sampling time with noise</i>	24
3.13	<i>Detailed view of the speed comparison in steady state for Figure 3.12</i>	25
3.14	<i>Simulation results without any noise and added offsets in the Measured and estimated speeds</i>	25
3.15	<i>Detailed view of the speed comparison in steady state for Figure 3.14</i>	26
3.16	<i>Simulation result comparison between Measured IM speed and EKF estimated speed for 20<math>\mu</math>s sampling time and observing the state of speed reversal with noise.</i>	26
3.17	<i>Detailed view of Figure 3.18 in the speed reversal region</i>	27
4.1	<i>Circuit schematic of the assembled circuit</i>	28
4.2	<i>Workplace and the assembled hardware</i>	31
4.3	<i>dSPACE control desk project UI</i>	32
5.1	<i>Loaded steady state operation of the motor</i>	33
5.2	<i>Detailed view of Figure 5.1 in the high-speed steady state region</i>	34

---

5.3	<i>Unloaded steady state operation of the motor.</i>	35
5.4	<i>Detailed view of Figure 5.3 in the high-speed steady state region</i>	35
5.5	<i>Comparison of loaded and unloaded operations mode in steady state</i>	36
5.6	<i>Varying Matrix <math>Q</math> while keeping <math>R</math> constant at 2000 in steady state</i>	37
5.7	<i>Varying Matrix <math>R</math> while keeping <math>Q</math> constant at 10</i>	38
5.8	<i>Varying Matrix <math>Q</math> while keeping <math>R</math> constant at 2000, for transient response</i>	38
5.9	<i>Comparison of rise time during transients for different <math>Q</math> values (<math>R = 2000</math>)</i>	39
5.10	<i>Comparison of fall time during transients for different <math>Q</math> values (<math>R = 2000</math>)</i>	39
5.11	<i>Unloaded Speed Reversal Transients with slew rate of 1.5</i>	40
5.12	<i>Comparison of loaded Speed Reversal Transients with slew rate of 0.05 and 1.5</i>	41
5.13	<i>Low-Speed performance with zero crossings (60 to -60</i>	42
5.14	<i>Measured and Estimated speed under varying loads with various speed references</i>	43

---

# *Abbreviations*

List of Abbreviations used in this thesis.

PE	Power Electronics
VFD	Variable Frequency Drives
IM	Induction Motor
KF	Kalman Filter
EKF	Extended Kalman Filter
PTC	Predictive Torque Control



---

# *Chapter 1*

## **Introduction**

The invention of Induction Motor was in 1888 by Nikola Tesla. This remarkable building up of a machine that didn't require brushes created a new sub stream in Electrical Engineering which gave rise to higher utilization of three-phase generation and distribution systems. Over the years as more electrical motors were developed, the mainstream uses of the induction motors were for the fixed speed operation while dc machines were utilized for the variable speed operations.

The variable speed operation used in dc machines using Ward-Leonard configuration requires 3 machine models (2 DC machines and 1 induction machine) making it more expensive and difficult for maintenance. But with the development of power electronic devices, there were variable speed drives for both DC and AC machines. The new power electronics (PE) components offered better torque speed and flux control than in the previous cases. With the development of Variable Frequency Drives (VFD) using new PE components, the new and better control schemes started to develop. There were developments of traditional Scalar controls like V/f control and new ones in the Vector control domains.

These days the development and research into the Vector control strategies are very extensive. While Direct Torque Control and Field Oriented Control inside the Vector control domain are predominant in the industrial scale with the high-performance electrical drive systems, Model Predictive Control strategies are gaining popularity too. The reasons for gaining popularity for the new control schemes while the existing ones are pretty effective being that, MPC usually has lower conceptual complexity[1] and the inclusion of the system constraints is easy along with lower cost function for the inner controller in the computation [1].

Even when applying these modern techniques they still require sensors for the minimal input conditions that give reference to the machine parameters. Those parameters being terminal voltages and currents and speeds. While the measurements of the voltages and currents are necessary factors the development of microprocessors and higher and compact computation devices have sparked and made possible the ideas for the sensorless

---

speed determination techniques. The sensorless vector controls of motor drives refer generally to the speed sensorless drives. The use of speed sensors is not always environmentally friendly. They are prone to large shocks and other environmental conditions [2]. The development of sensorless control and predictive analysis is effective from the perspective of reliability, and maintainability. The sensorless controls are more robust in contrast to the use of sensors in other methods. In addition to this, the economic aspects of the sensorless controls are more desirable [3].

Primary aspects of the sensorless control are the estimation of the rotor speed using predictive filter algorithms, and coupling the estimated speed with the MPC strategies. In this thesis, we present the derivation, implementation and hardware realization of one of such methods of sensorless control using Kalman Filter techniques, in a laboratory motor and the comparison of such a filter response with the actual response and the references given. The primary task discussed in this thesis includes the design and implementation of the Kalman Filter and the reliability of the estimated speed, in comparison with the actual motor speed and the reference speed. The further extension of the estimated speed has been on the deployment of the sensorless vector control of the motor. But the thesis primarily focusses on the estimation of the rotor speed. We are starting with the mathematical modeling of the filter and the machine models used in this thesis in Chapter 2. In Chapter 3, we will discuss the Simulation of the filter and the motor model and control strategies in Matlab Simulink. Chapter 4 discusses the workplace setup and the hardware assembled to realize the model verified in the simulations to the laboratory. In Chapter 5 the various experimental results are analyzed. Chapter 6 is the Conclusion for the thesis. Following sections after it is the References.



---

## Chapter 2

# Kalman Filter and its Design for Induction Motor Speed Determination

### 2.1 Kalman Filter:

The estimation of the rotor speed in this thesis focuses on the Kalman Filter and Extended Kalman Filter. The Kalman Filter (KF) is a mathematical tool for estimation of a state based on the previous state and the observed values of the noise like measurement noise and the system noise and measured values – like outputs. They are primarily used in prediction and estimation fields that include GPS operations, AI applications where positioning and band of errors are significant, and unmanned operations like space and military operations.

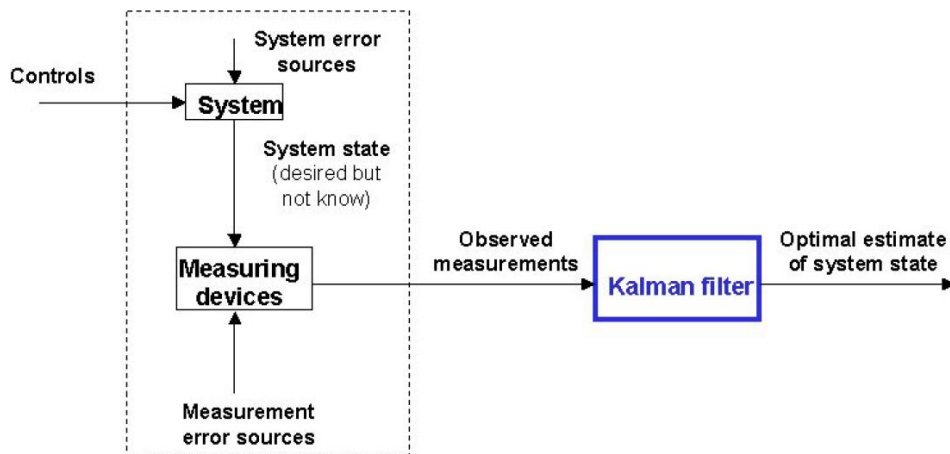


Figure 2.1: Typical application of Kalman Filter

The KF operates in 2 repeating steps, the prediction and correction states. The initial prediction stage estimates a value of the desired state from the inputs and previous state variables. Then the uncertainty of the estimated value is calculated from the difference between previous prediction and the measured reality. This uncertainty is regarded not to change within the current sample. The predicted state variable are then corrected accordingly. This process of prediction and correction produces the final estimated values to be closer to the real values.

---

### 2.1.1 The Process to be estimated:

KF is used in the estimation of a discrete-time controlled process that is governed by the linear stochastic difference equation. [4]

$$x_k = Fx_{k-1} + B_k u_{k-1} + v_{k-1} \quad (2.1)$$

And the output (observation) given by

$$y_k = H_k x_k + w_k \quad (2.2)$$

Where,

$$p(v) \sim N(0, Q) \quad (2.3)$$

$$p(w) \sim N(0, R) \quad (2.4)$$

Where,  $u_k$  represents the input parameter or the control vector,  $F_k$  is the state transition model,  $B_k$  is the control input model, and  $H_k$  is the observation model which maps the true state space into the observed space or the output. The random variables  $w_k$  and  $v_k$  in equations 2.1 and 2.2 represent the process and measurement noise respectively. The noises are uncorrelated, assumed to be white noise with normal probability distributions. The  $Q$  and  $R$  are the system noise covariance matrix and measurement noise covariance matrix. While they are changing constantly in every time step and measurement, it is assumed that they are constant matrices. [4]

### 2.1.2 The Estimation Process:

Like we described earlier the filtering process occurs over two stages: prediction and correction. The initial conditions for the first stage are given with the prior knowledge of the process to be estimated or state as we would call it here forward, and the state covariance matrix of prediction ( $P$ ). The first stage initializes the state vectors and the covariance matrices, then the preliminary prediction of the state vector and the covariance matrix of prediction. On the second stage of the loop, which is the correction stage, the measurement noise covariance matrices come into play. Initially, the Kalman Gain is computed based on the predicted  $P$  in the first stage, along with the inclusion of measurement noise in the equation. After the calculation of the Kalman Gain, the state vector predicted in the first stage are corrected based on the error factor developed from the difference of the measured and predicted outcome values. Then the correction of the covariance matrix of prediction is done for the next loop which acts as the initial condition

---

for the next loop. In this way, the 2 stage loop cycle runs to give an estimate for any discrete-time controlled process governed by the linear stochastic difference equation.[4]

### 2.1.3 Mathematical Representation:

#### Predict:

$$\text{Predicted State:} \quad \hat{x}_{k|k-1} = F_k \hat{x}_{k-1|k-1} + B_k u_k \quad (2.5)$$

$$\text{Covariance of Prediction} \quad P_{k|k-1} = F_k P_{k-1|k-1} F_k^T + Q_k \quad (2.6)$$

#### Update:

$$\text{Kalman Gain Computation:} \quad K_k = P_{k|k-1} H_k^T (H_k P_{k|k-1} H_k^T + R_k)^{-1} \quad (2.7)$$

$$\text{Measurement residual:} \quad \tilde{y}_k = y_k - H_k \hat{x}_{k|k-1} \quad (2.8)$$

$$\text{Updated state estimate:} \quad \hat{x}_{k|k} = \hat{x}_{k|k-1} + K_k \tilde{y}_k \quad (2.9)$$

$$\text{Updated Covariance of Prediction} \quad P_{k|k} = (I - K_k H_k) P_{k|k-1} \quad (2.10)$$

## 2.2 Extended Kalman Filter:

The Kalman Filter discussed above is only valid for linear functions, while most of the real systems are governed by non-linear functions. The Extended Kalman Filter (EKF) is the nonlinear version of the Kalman Filter. It linearizes about the current mean and covariance. [5] While EKF had been used extensively as a standard tool for estimation of nonlinear states in navigation systems and GPS, with the introduction of Unscented Kalman Filter the extensive use has reduced. [6]

In the modeling of the filter in this thesis, the Extended Kalman Filter algorithm has been used. The difference in the formulation of the EKF in comparison to KF is such that the state transition and observation state space models may not be linear functions of the state but are often many nonlinear functions. [7]

$$x_k = f(x_{k-1}, u_k) + v_k \quad (2.11)$$

$$y_k = h(x_k) + w_k \quad (2.12)$$

Like in the previous case with KF the random variables  $v_k$  and  $w_k$  are the system and measurement noises, which are both assumed to be zero mean multivariate Gaussian noise with covariance  $Q_k$  and  $R_k$  respectively. The vector  $u_k$  is the input control vector.

---

The functions  $f$  and  $h$  each compute the predicted states using the data from the previous estimate and predicted measurement from predicted state respectively. Because of the nonlinear state of the model being applied, they cannot be applied directly to the covariances. To solve this, a Jacobian is computed for both the functions with the current predicted states. By creating the Jacobians for the covariances, the non-linear function is linearized around the current estimate and the matrices can be used in the Kalman Filter equations.

### 2.2.1 Mathematical Representation:

The mathematical representation is slight different from the original one in the Extended Kalman Filter due to the Jacobian calculations. They are presented below:

#### Predict:

$$\text{Predicted State:} \quad \hat{x}_{k|k-1} = f(\hat{x}_{k-1|k-1}, u_k) \quad (2.5)$$

$$\text{Covariance of Prediction} \quad P_{k|k-1} = F_k P_{k-1|k-1} F_k^T + Q_k \quad (2.6)$$

#### Update:

$$\text{Kalman Gain Computation:} \quad K_k = P_{k|k-1} H_k^T (H_k P_{k|k-1} H_k^T + R_k)^{-1} \quad (2.7)$$

$$\text{Measurement residual:} \quad \tilde{y}_k = y_k - h(\hat{x}_{k|k-1}) \quad (2.8)$$

$$\text{Updated state estimate:} \quad \hat{x}_{k|k} = \hat{x}_{k|k-1} + K_k \tilde{y}_k \quad (2.9)$$

$$\text{Updated Covariance of Prediction} \quad P_{k|k} = (I - K_k H_k) P_{k|k-1} \quad (2.10)$$

Where the state transition and output observation matrices,  $F_k$  and  $H_k$  are defined as following Jacobians,

$$F_k = \left. \frac{\partial f}{\partial x} \right|_{\hat{x}_{k-1|k-1}, u_k} \quad (2.11)$$

$$H_k = \left. \frac{\partial h}{\partial x} \right|_{\hat{x}_{k|k-1}} \quad (2.12)$$

## 2.3 Mathematical Model of the Induction Motor

For the simulation of the motor model, a dynamic model expressed in the stator flux oriented reference frame was chosen. In this modeling, the state variables are chosen

as stator currents  $i_{ds}$ ,  $i_{qs}$ , and the rotor flux  $\varphi_{dr}$ ,  $\varphi_{qr}$  as state variables. The state space representation of such a model can be written as:

$$\frac{dX(t)}{dt} = A * X(t) + B * u(t) \quad (2.13)$$

$$Y(t) = C * X(t) \quad (2.14)$$

Where,

$$X = [i_{ds} \ i_{qs} \ \varphi_{dr} \ \varphi_{qr}]^T \quad (2.15)$$

$$Y = [i_{ds} \ i_{qs}]^T \quad (2.16)$$

$$u = [v_{ds} \ v_{qs}]^T \quad (2.17)$$

$$A = \begin{bmatrix} -\left(\frac{R_s}{\sigma L_s} + \frac{1-\sigma}{\sigma \tau_r}\right) & 0 & \frac{L_m}{\sigma L_s L_r} \frac{1}{\tau_r} & \omega_r \frac{L_m}{\sigma L_s L_r} \\ 0 & -\left(\frac{R_s}{\sigma L_s} + \frac{1-\sigma}{\sigma \tau_r}\right) & -\omega_r \frac{L_m}{\sigma L_s L_r} & \frac{L_m}{\sigma L_s L_r} \frac{1}{\tau_r} \\ \frac{L_m}{\tau_r} & 0 & -\frac{1}{\tau_r} & -\omega_r \\ 0 & \frac{L_m}{\tau_r} & \omega_r & \frac{1}{\tau_r} \end{bmatrix}$$

$$B = \begin{bmatrix} \frac{1}{\sigma L_s} & 0 \\ 0 & \frac{1}{\sigma L_s} \\ 0 & 0 \\ 0 & 0 \end{bmatrix}$$

$$C = \begin{bmatrix} 1 & 0 & 0 & 0 \\ 0 & 1 & 0 & 0 \end{bmatrix}$$

Where,

$R_s$  = Stator Resistance (ohm)

$R_r$  = Rotor Resistance (ohm)

$L_s$  = Stator self-inductance (H)

$L_r$  = Rotor self-inductance (H)

$L_m$  = Mutual inductance (H)

$\sigma = 1 - \frac{L_m^2}{L_s L_r}$  = leakage coefficient

$\tau_r = \frac{L_r}{R_r}$  = rotor time constant

$\omega_r$  = motor angular velocity (rad/s)

---

## 2.4 Designing and Implementing the EKF to the Motor Model:

### 2.4.1 Extension of the state vector to add rotor angular speed as a state variable:

In the above dynamic model of the Induction Motor, if we include the rotor angular speed as one of the state variables the model becomes nonlinear.[8] With the inclusion of the rotor angular speed as one of the state variables the equations above change in the following ways:

$$X = [i_{ds}^s \quad i_{qs}^s \quad \varphi_{dr}^s \quad \varphi_{qr}^s \quad \omega_r]^T \quad (2.21)$$

$$Y = [i_{ds}^s \quad i_{qs}^s]^T = i_s \quad (2.22)$$

$$u = [V_{ds}^s \quad V_{qs}^s]^T \quad (2.23)$$

$$A =$$

$$\begin{array}{ccccc|c} -\frac{1}{T_s^*} & 0 & \frac{L_m}{L'_s L_r} \frac{1}{\tau_r} & \omega_r \frac{L_m}{L'_s L_r} & 0 & \\ 0 & -\frac{1}{T_s^*} & -\omega_r \frac{L_m}{L'_s L_r} & \frac{L_m}{L'_s L_r} \frac{1}{\tau_r} & 0 & \\ \frac{L_m}{\tau_r} & 0 & -\frac{1}{\tau_r} & -\omega_r & 0 & \\ 0 & \frac{L_m}{\tau_r} & \omega_r & \frac{-1}{\tau_r} & 0 & \\ 0 & 0 & 0 & 0 & 0 & \end{array}$$

$$B = \begin{bmatrix} \frac{1}{\sigma L_s} & 0 \\ 0 & \frac{1}{\sigma L_s} \\ 0 & 0 \\ 0 & 0 \\ 0 & 0 \end{bmatrix} \quad C = \begin{bmatrix} 1 & 0 & 0 & 0 & 0 \\ 0 & 1 & 0 & 0 & 0 \end{bmatrix}$$

Where,

$$\frac{1}{T_s^*} = \frac{R_s + R_r \left(\frac{L_m}{L_r}\right)^2}{L'_s} \quad (2.24)$$

$$L'_s = \sigma L_s \quad (2.25)$$

---

### 2.4.2 Discretization of the IM Model:

Because of the nonlinearity of the model, the designing of the EKF becomes important. But for the implementation of the EKF, the discretization of the IM model equations are required. Discretizing the IM model equation above we get the following equations:

$$X_k = A_d X_{k-1} + B_d u_{k-1} \quad (2.26)$$

$$Y_{k-1} = C X_{k-1} \quad (2.27)$$

$$A_d \approx I + AT \quad (2.28)$$

$$B_d \approx BT \quad (2.29)$$

$A_d =$

$$\begin{pmatrix} 1 - \frac{T}{T_s^*} & 0 & \frac{TL_m}{L'_s L_r \tau_r} & \frac{\omega_r TL_m}{L'_s L_r} & 0 \\ 0 & 1 - \frac{T}{T_s^*} & -\frac{\omega_r TL_m}{L'_s L_r} & \frac{TL_m}{L'_s L_r \tau_r} & 0 \\ \frac{TL_m}{\tau_r} & 0 & 1 - \frac{T}{\tau_r} & -T\omega_r & 0 \\ 0 & \frac{TL_m}{\tau_r} & T\omega_r & 1 - \frac{T}{\tau_r} & 0 \\ 0 & 0 & 0 & 0 & 1 \end{pmatrix}$$

The sampling time used in the discretization plays a relatively very important role in obtaining accurate results. This will be discussed more in detail in the simulation and experimental design sections. Usually smaller sampling time corresponds to lower cyclic loops of the EKF and better accuracy, while it is important to note that the sampling time shouldn't be shorter than the time taken for implementation of each loop in EKF algorithm. The compromise between accuracy and stability is needed during the sampling time assessment.

The system noise is given as  $v_k$  which is assumed to be zero mean white Gaussian noise, independent of the state vector and has covariance matrix  $Q$ . The system model after this is represented as:

$$X_k = A_d X_{k-1} + B_d u_{k-1} + v_{k-1} \quad (2.30)$$

---

Similarly, the measurement noise is given as  $w_k$  which is assumed to be zero mean white Gaussian noise, independent of the state vector and the system noise and has a covariance of R. The output model after this is represented as:

$$Y_{k-1} = C X_{k-1} + w_{k-1} \quad (2.31)$$

### 2.4.3 Determination of the Noise and State Covariance Matrices

The System Noise and Measurement Noise covariance matrices Q and R have element numbers that are varying based on the number of state variables.[8] The matrix Q is a five-by-five matrix because of 5 state variables and R is two-by-two matrix because of 2 output states. But since it is assumed that there is no correlation between the noises, we can assume both the covariance matrices to be diagonal matrices. This assumption reduces the complexity of the calculation.

The noise matrices are important for initialization because the idea of KF depends on the inclusion of the noise factors to get a very approximate estimate of the estimated quantity. In our model, the direct and quadrature axes parameters are usually the same, that further reduces the complexity in the calculation and initialization of the covariance matrices, where ( $q_{11}=q_{22}$ ,  $q_{33}=q_{44}$ ,  $r_{11}=r_{22}$ ). This reduced complexity helps us define the noise matrices with just 4 variables like shown below.

$$Q = \begin{bmatrix} q_{11} & 0 & 0 & 0 & 0 \\ 0 & q_{11} & 0 & 0 & 0 \\ 0 & 0 & q_{33} & 0 & 0 \\ 0 & 0 & 0 & q_{33} & 0 \\ 0 & 0 & 0 & 0 & q_{55} \end{bmatrix} \quad R = \begin{bmatrix} r & 0 \\ 0 & r \end{bmatrix}$$

### 2.4.4 Implementation of EKF Algorithm:

The discretized model of the machine and the implementation of the EKF algorithm looks like as shown in Fig 2.3, in the modular block representation. The representation is divided into two sections the Machine Model with the continuous time domain and the EKF model with the discrete time domain. The interaction between the two models and their separation is shown with the dotted line.



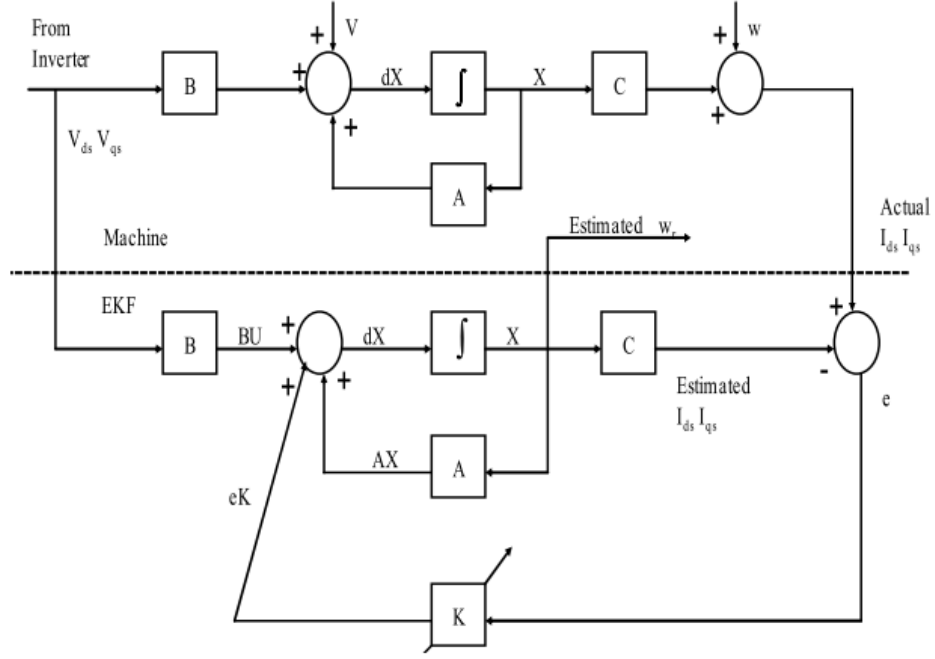


Figure 2.2: Structure of EKF [2]

#### 2.4.4.1 Initialization of state vectors and covariance matrices

At the beginning, all the initializing values for the state vector is  $X_0 = X(t_0)$  and the noise covariance matrices are  $Q_0(5 \times 5)$  and  $R_0(2 \times 2)$ . The initial values of  $Q$  and  $R$  are selected randomly. The filter requires the tuning of the  $Q$  and  $R$  according to the mode of operation, this is discussed in more detail in Chapter 3. And the state covariance matrix initialized at  $P_0(5 \times 5)$ . The state covariance matrix is considered a diagonal matrix with all elements same for the initialization.

#### 2.4.4.2 Prediction of the state variable

The state variable is predicted for the sampling time instant ( $k$ ) is obtained from the input  $u_{k-1}$  and the state vector  $\hat{X}_{k-1}$ .

$$X_k^* = A_d \hat{X}_{k-1} + B_d u_{k-1} \quad (2.32)$$

Where,

$$\hat{X}_{k-1} = [\hat{i}_{ds|k-1} \quad \hat{i}_{qs|k-1} \quad \hat{\varphi}_{dr|k-1} \quad \hat{\varphi}_{qr|k-1} \quad \hat{\omega}_r|k-1]^T \quad (2.33)$$

$$u_{k-1} = [V_{ds|k-1} \quad V_{qs|k-1} \quad 0 \quad 0 \quad 0]^T \quad (2.34)$$

### 2.4.4.3 Estimation of the Covariance Matrix of Prediction:

The covariance matrix of prediction is estimated as

$$P_k^* = F_k \hat{P}_{k-1} F_k^T + Q \quad (2.36)$$

here the function  $F$  is the Jacobian (gradient function) of the system model function described earlier that linearizes the model. The function  $F$  is defined as

$$F_k = \left. \frac{\partial}{\partial x} [A_d X + B_d u] \right|_{x = \hat{x}_{k-1}, u_{k-1}} \quad (2.37)$$

$F_k =$

$$\begin{pmatrix} 1 - \frac{T}{T_s^*} & 0 & \frac{TL_m}{L'_s L_r \tau_r} & \frac{\omega_r TL_m}{L'_s L_r} & \frac{TL_m}{L'_s L_r} \varphi_{qr} \\ 0 & 1 - \frac{T}{T_s^*} & -\frac{\omega_r TL_m}{L'_s L_r} & \frac{TL_m}{L'_s L_r \tau_r} & -\frac{TL_m}{L'_s L_r} \varphi_{dr} \\ \frac{TL_m}{\tau_r} & 0 & 1 - \frac{T}{\tau_r} & -T\omega_r & T\varphi_{qr} \\ 0 & \frac{TL_m}{\tau_r} & T\omega_r & 1 - \frac{T}{\tau_r} & T\varphi_{dr} \\ 0 & 0 & 0 & 0 & 1 \end{pmatrix}$$

Where,

$$\omega_r = \hat{\omega}_{r|k} \quad \varphi_{dr} = \hat{\varphi}_{dr|k} \quad \varphi_{qr} = \hat{\varphi}_{qr|k}$$

### 2.4.4.4 Kalman Gain computation

The Kalman gain matrix is a five-by-two matrix for this model of IM we are modeling. And is given by the following formula that includes the measurement noise parameters as well.

$$K_k = P_k^* H_k^T (H_k P_k^* H_k^T + R_k)^{-1} \quad (2.38)$$

here the function  $H_k$  is the Jacobian (gradient function) of the output model function described earlier that linearizes the model. The function  $H_k$  is defined as

$$H_k = \left. \frac{\partial}{\partial x} [C_d X] \right|_{x_k = \hat{x}_k^*} \quad (2.39)$$

$$H_k = \begin{bmatrix} 1 & 0 & 0 & 0 & 0 \\ 0 & 1 & 0 & 0 & 0 \end{bmatrix}$$

---

#### 2.4.4.5 State Vector Estimation:

The final estimated state vector and the output models after the filtering at time (k+1) is given as:

$$\hat{X}_k = X_k^* + K_k \tilde{Y}_k \quad (2.40)$$

$$\tilde{Y}_k = Y_k - \hat{Y}_k \quad (2.41)$$

$$\hat{Y}_k = C_d X_k^* \quad (2.42)$$

#### 2.4.4.6 Correction of the Covariance Matrix of Prediction for next loop:

The error covariance matrix is obtained from

$$\hat{P}_k = P_k^* - K_k H_k P_k^* \quad (2.43)$$

With the last step the loop ends for 1 cycle, for the next sampling time instant that is k+1, now the values in the loop are updated by putting k = k+1, and repeating the process from 2.4.4.2 to 2.4.4.6.

---

## Chapter 3

### Simulation of IM and EKF in Simulink Matlab

In the previous chapter, we developed the mathematical modeling of the EKF and the IM equations for the estimation of the rotor speed. In this chapter, we will continue with mapping those equations into the Matlab Simulink and look at the preliminary simulation results.

#### 3.1 Model of IM and Control Strategy:

The following model of the IM used in this thesis simulation is helped to develop by **Mr. Pavel Karlovsky**. The motor drive control strategy used in this simulation includes Predictive Torque Control which is one of the categories of Model Predictive Control (MPC). They are the most commonly used motor drives in sync with the sensorless motor drive controls. The Simulink Model of the IM, Control strategies and the inclusion of the Filter Block developed is given below:

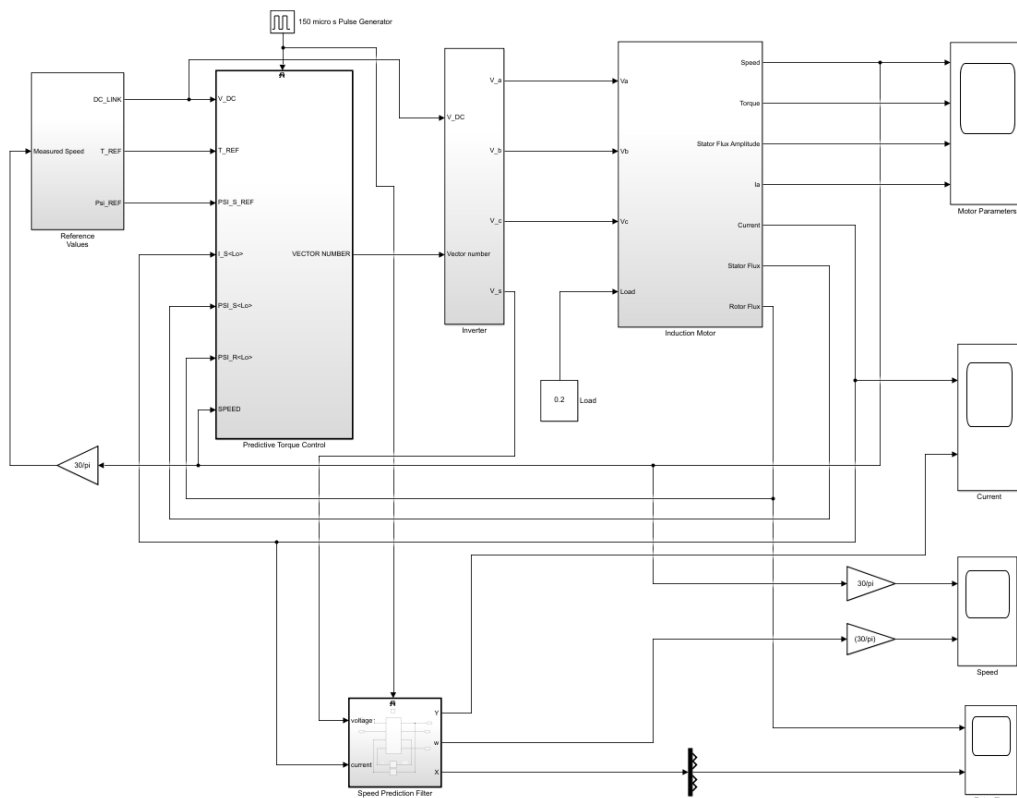


Figure 3.1: Simulink Model of the estimation of rotor speed of IM with the control mechanism

The major blocks in this simulation include the Reference Block, Predictive Torque Control Block, Inverter Block, Induction Motor Block (from left to right on Figure 4.1 on the top shelf) and the EKF block at the bottom. Each of the Blocks internal schematic are discussed ahead.

### 3.1.1 Reference Values Block

In this block the DC-Link voltage reference values, Flux Reference and the Torque reference with the PID controller that gives torque output, with the limitation to 5 Nm, with the comparison between the Reference Values of the Speed and the Measured Speed Value. The Reference Values are forwarded to the Predictive Torque Control Block.

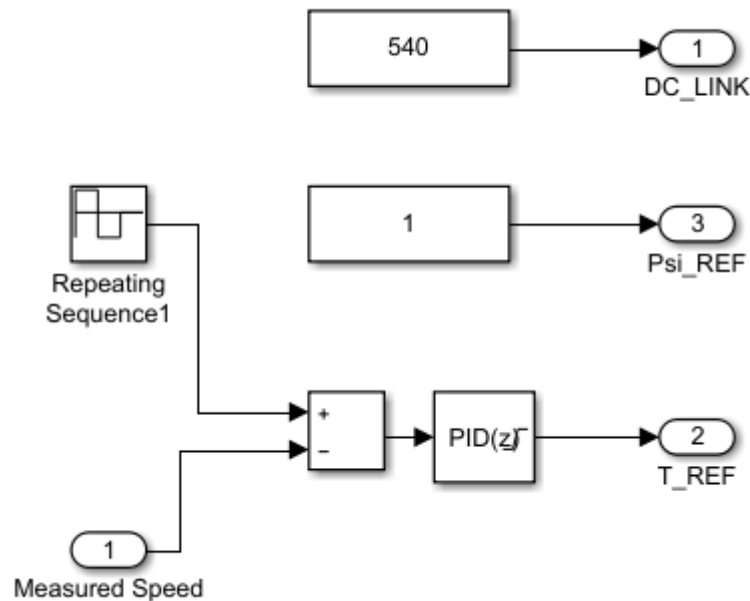


Figure 3.2: Reference Values Block

### 3.1.2 Predictive Control Block

In this block, the Predictive Torque Control (PTC) for the motor drive is employed, it employs the prediction and the cost function block which sends the selected vector signal from the calculated cost function from the prediction to the Inverter Block next to it. The schematic of the model is presented below along with the cost function equation.

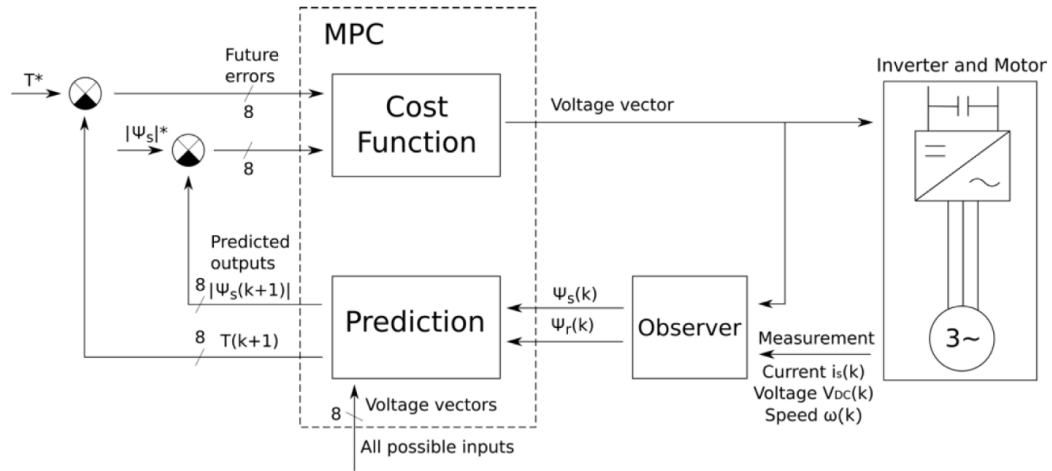


Figure 3.3: Block diagram schematic of IM drive Model Predictive Control [10]

The Cost function  $g$  is given by:

$$g(n) = k * \left| |\varphi_s(k+1)| - |\varphi_s|^* \right| + |T(k+1) - T^*| \quad (3.1)$$

Where, 
$$k = \frac{T_n}{|\varphi_n|} \quad (3.2)$$

Here, the coefficient  $k$  in equation 3.1 determines, what impact the two part of the equation have on the resulting value. It is chosen as a fraction of nominal torque and nominal flux amplitude of the motor as shown in equation 3.2 [10]

### 3.1.3 Inverter Block

The topology of the inverter and the vector selection based on the vector number from the previous block is presented here. This also includes the  $\alpha\beta$  to abc transformation block in the end section. The figurative representation of the voltage selection diagram and the equation is presented below in Fig: 3.4.

In accordance with the Fig 3.4, the voltage equation becomes:

$$V_s = \frac{2}{3} * V_{DC} * (V_{x\alpha} + jV_{x\beta}) \quad (3.3)$$

Here,  $V_s$  = stator voltage

$V_{DC}$  = DC link voltage

$V_{x\alpha}, V_{x\beta}$  = the alpha and beta components of the selected voltage vector

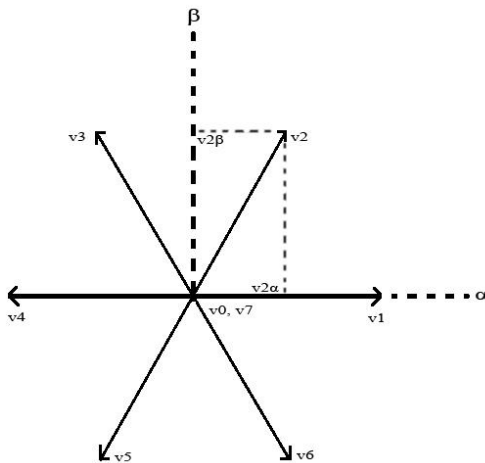


Figure 3.4: Voltage vector diagram

### 3.1.4 IM Model Block

The IM motor model block has a lot of sub blocks constructed inside it. The modeling of the IM is based on the IM equations of rotor flux and stator currents and also the moment and torque calculations. The first overview of the IM block is given below:

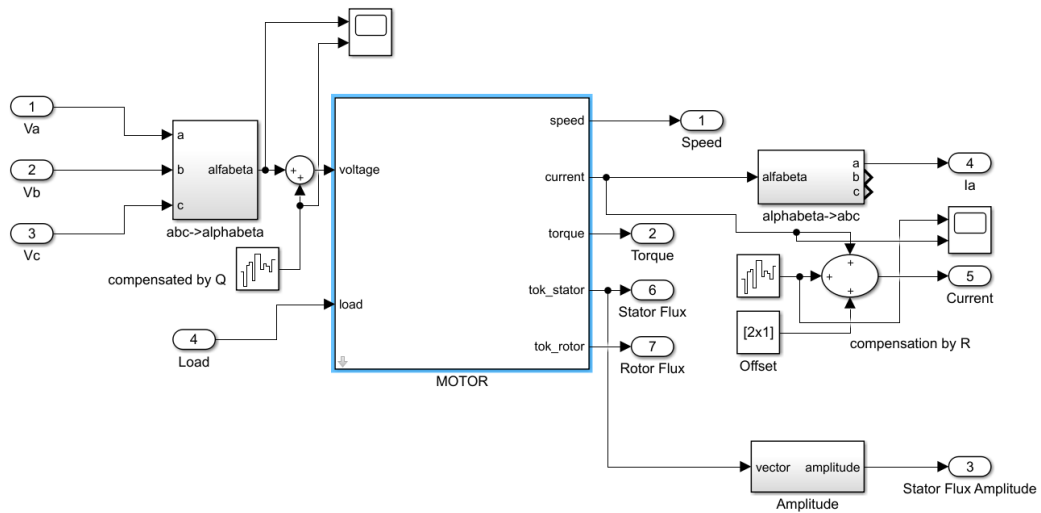


Figure 3.5: IM block representation

The parameters of the motor used in the simulation have been based on the laboratory motor model available. The motor parameters used in the simulation are listed in the appendix along with the two axis model IM equations.

### 3.2 EKF Model

The bottom block in Figure 3.1 corresponds to the EKF Block. The primary input variables to the EKF block are the terminal voltage and currents. They are extracted from the Inverter and the Induction Motor output ports. While in the laboratory setup they are analyzed by sensors and fed to the microprocessor unit that operates the filter algorithm and its computations. The internal schematics of the block are given below.

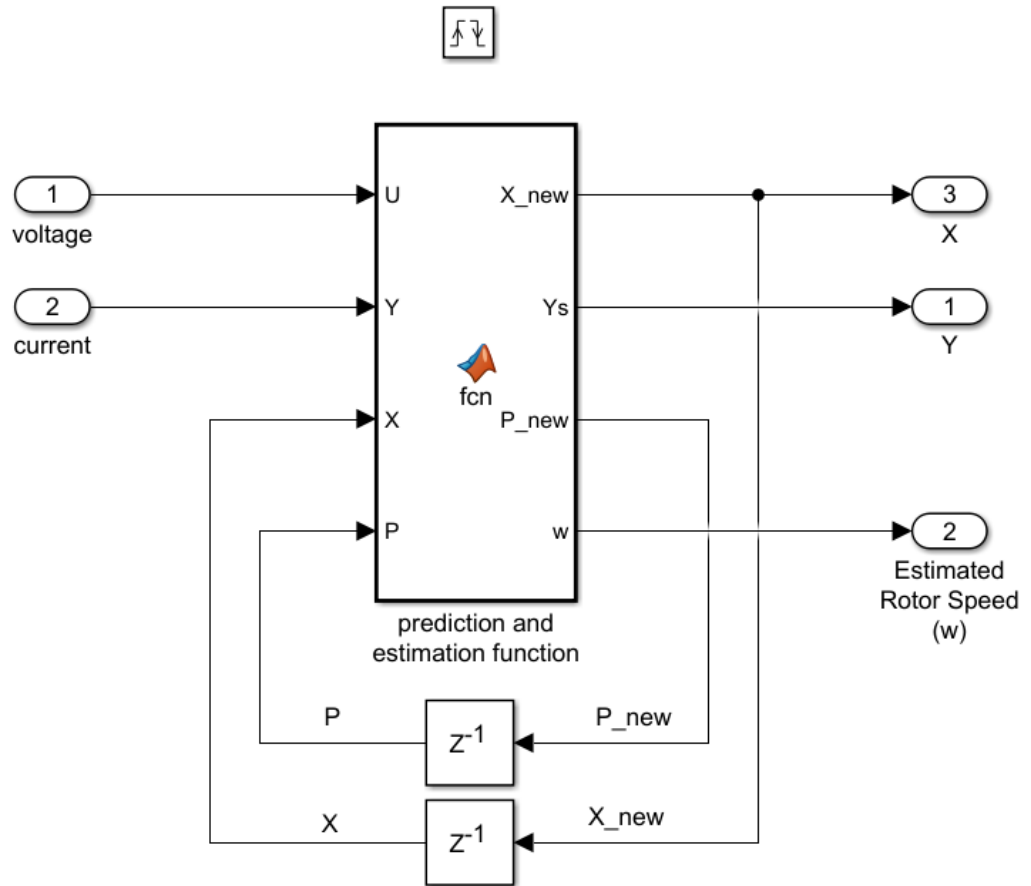


Figure 3.6: EKF block

#### 3.2.1 EKF algorithm

As discussed in the previous chapter the EKF algorithm is modeled in the EKF block for the prediction and estimation. The algorithm takes terminal voltages and current from machine model, and the other inputs are state vector matrix and covariance matrix of estimation or state covariance matrix. It returns the new predicted state vector, Predicted Output and the updated state covariance matrix and the estimated rotor speed. The algorithm developed and written in Matlab is presented below:



---

```

function [X_new,Ys,P_new,w] = fcn(U,Y, X,P)

%motor constants
Lsr=0.63866;
Ls=Lsr+0.04621;
Lr=Lsr+0.04986;
Rs=10.79;
Rr=6.674;

%user defined working variables
Ts = 15e-5;
kr = Lsr/Lr;
R_sigma = Rs+Rr*kr*kr;
sigma = 1-Lsr*Lsr/Ls/Lr;
tau_sigma = (sigma*Ls)/R_sigma; %T*s variable
tau_r = Lr/Rr;
pp =2;

Lss = sigma*Ls;
%for 5*5 we need to define w from the existing variable
w = X(5,1);

%Discretized A
A = [(1-Ts/tau_sigma)    0      Ts*Lsr)/(Lss*Lr*tau_r)
      w*(Ts*Lsr)/(Lss*Lr)    0;
      0      1-(Ts/tau_sigma)  -w*(Ts*Lsr)/(Lss*Lr)
      (Ts*Lsr)/(Lss*Lr*tau_r) 0;
      (Ts*Lsr)/tau_r    0      1-(Ts/tau_r)      -Ts*w 0;
      0      (Ts*Lsr)/tau_r    Ts*w  1-(Ts/tau_r)    0;
      0      0      0      0      0      1];

%Discretized B
B = [ Ts/Lss    0;
      0      Ts/Lss;
      0      0;
      0      0;
      0      0];

C = [ 1  0  0  0  0;
      0  1  0  0  0];

Q = [ 0  0  0  0  0;
      0  0  0  0  0;
      0  0  0  0  0;
      0  0  0  0  0;
      0  0  0  0  10];

R = [ 2000  0
      0    2000];
%H is the gradient matrix (Jacobian) of the output function
H = [ 1  0  0  0  0;
      0  1  0  0  0];

X_mid = A*X+B*U; %for 5x5 this variable is X_mid
Ys = C*X_mid;

```

---

```

w_mid = X_mid(5,1);
phi_dr = X_mid(3,1);
phi_qr = X_mid(4,1);

%F is the gradient matrix(Jacobian) of the state matrix or state
function
F = [(1-Ts/tau_sigma)    0    (Ts*Lsr)/(Lss*Lr*tau_r)
      w_mid*(Ts*Lsr)/(Lss*Lr)  phi_qr*(Ts*Lsr)/(Lss*Lr);
      0    1-(Ts/tau_sigma)  -w_mid*(Ts*Lsr)/(Lss*Lr)
      (Ts*Lsr)/(Lss*Lr*tau_r)  -phi_dr*(Ts*Lsr)/(Lss*Lr);
      (Ts*Lsr)/tau_r    0    1-(Ts/tau_r)  -Ts*w_mid    Ts*phi_qr;
      0    (Ts*Lsr)/tau_r    Ts*w_mid    1-(Ts/tau_r)    Ts*phi_dr;
      0    0    0    0    1];

P_mid = F*P*F' + Q; % Covariance matrix of prediction

K = P_mid*H'*(inv(H*P_mid*H' + R)); %Kalman Gain

P_new = P_mid - K*H*P; %Updating of the covariance matrix

X_new = X_mid + K*(Y-Ys); %Here Y is the actual measured value
obtained
%and Ys is the calculated value from filter

w = X_new(5,1)/pp;

```

### 3.2.2 Tuning of the noise covariance matrices Q and R

In the above results, we can see that the  $150 \mu\text{s}$  sampling time results have lower oscillation amplitudes and the lower sampling items have higher oscillation amplitudes. This is due to the different tuning of the EKF by changing the values inside the noise covariance matrix Q and R. Changing the values of these covariance matrices changes both the steady-state performance and the transient performance of the filter. For the simplicity of the simulation, we have assumed the machine model is ideal so the value in the first 4 diagonal components in the Q matrix is assumed 0 ( $q_{11} = q_{22} = q_{33} = q_{44} = 0$ ) and only the noise in the last diagonal element ( $q_{55}$ ) is assumed. The two diagonal elements in R matrix are equal ( $r_{11} = r_{22}$ ) as well in all the further calculation as discussed earlier in chapter 2. Also, in all of the experimentation through, only  $q_{55}$ , and  $r_{11}$  and  $r_{22}$  are changed during tuning. The tuning of the values of R and Q changes the stability of the filter and the occurrence of the ripples and the amplitude of the ripples. In low sampling times, the mean value of the estimate is closer to the real value but the fluctuations are higher as seen above. While in higher sampling values the offset is higher but the ripples are small. The balance

---

between the stability and the oscillations has to be selected. Between the values of  $Q$  and  $R$ , the change in  $Q$  denotes the uncertainty in the machine model used and  $R$  denotes the level of noise in the measurements. Higher  $Q$  corresponds to higher uncertainty in the machine model used hence higher system noise. Higher  $R$  corresponds to higher measurement noise, and the filter subjects them to less weight during computation. Hence higher  $R$  causes longer computation time, making the transient performance slower. The matrices have been tuned on various cases accordingly, based on the sampling time used and the machine performance being observed is a transient response or steady state.

### **3.3 Simulation Results from Matlab Simulink**

The simulation of the above model and the filter algorithm for the parameters of the laboratory IM is done. The simulation was done for multiple sampling times (20  $\mu$ s, and 150  $\mu$ s). The simulation results are presented below. Figure 3.7 shows the graphical representation of the induction motor run over time, as we start the motor from a standstill and take it to 1500rpm. At 6s, the motor stands to decelerate from 1500rpm to reach rotor speed of 1000rpm. The variations in the rotor speed, the torque generated by the motor, Stator flux amplitude and one of the phase currents is seen. Because the simulated was tried to represent as much as the real model the addition of white noise to both current and voltages have been done in the simulations both at 10% of the peak levels of individual quantities respectively and relatively high offset level of 1A was added accordingly.

Figure 3.8 shows the simulation results of the EKF predicted output current compared to the current from the IM. In both cases, only one of the phases is shown for graphical clarity.

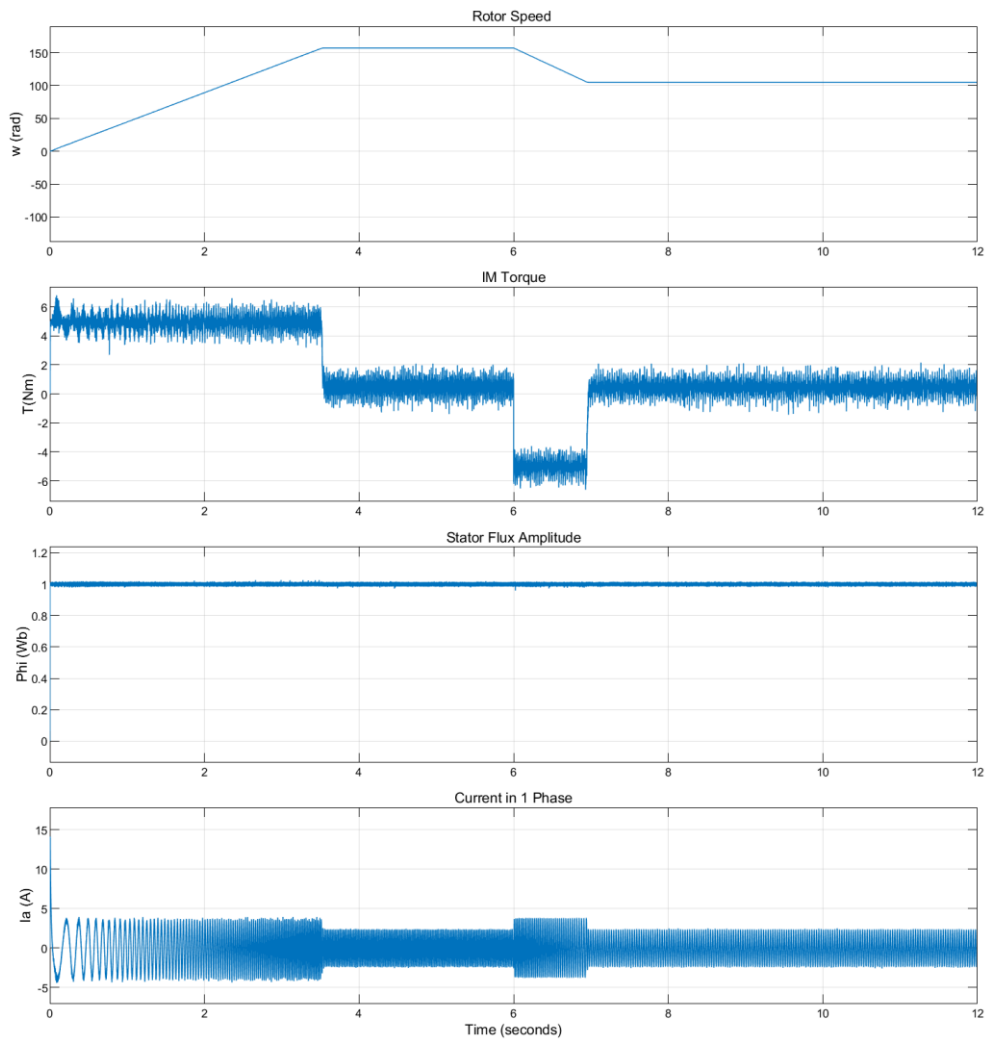


Figure 3.7: Simulation Results of the IM parameters.

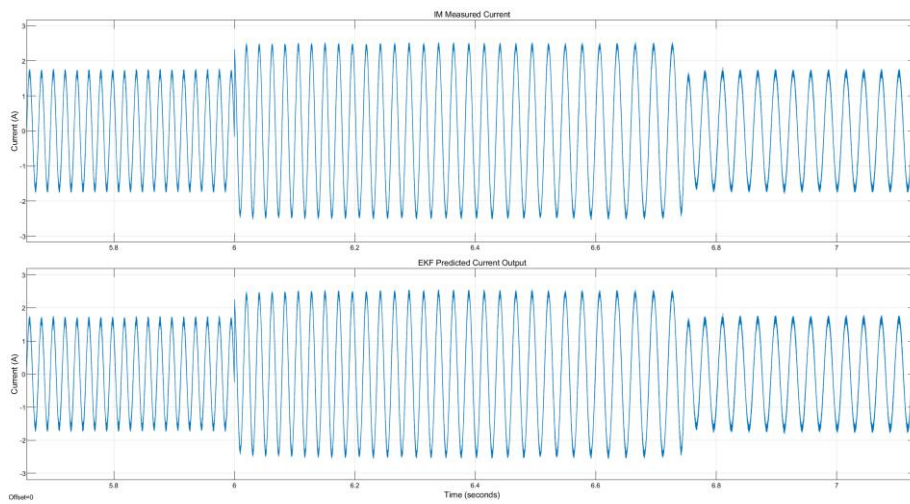


Figure 3.8: Comparison of IM Measured Current and EKF estimated Current

Figure 3.9 shows the simulation results of the EKF estimated Rotor Flux and the Rotor Flux as seen from the IM. In both cases, only one of the phases is shown for graphical clarity.

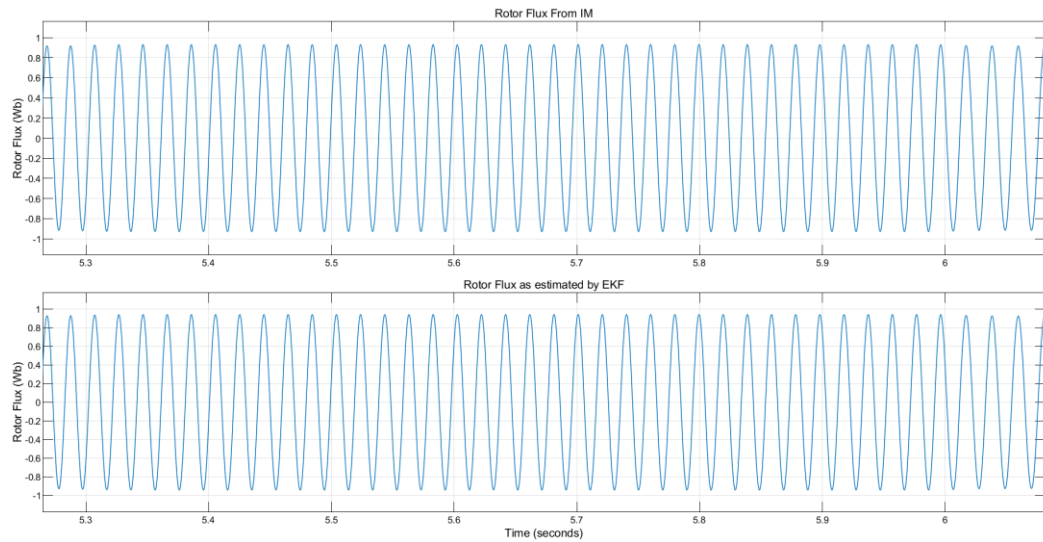


Figure 3.9: Comparison of IM Measured Rotor Flux and EKF estimated Rotor Flux

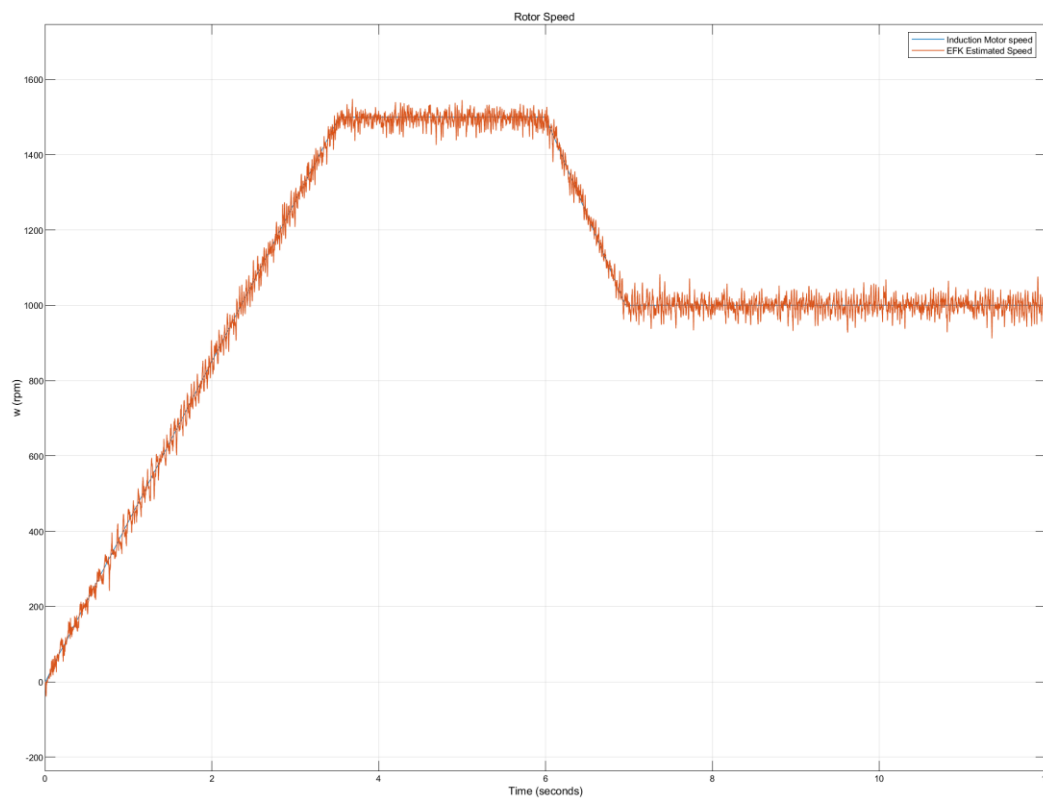


Figure 3.10: Simulation comparison between Measured IM speed and EKF estimated speed for  $20 \mu\text{s}$  sampling time with noise.

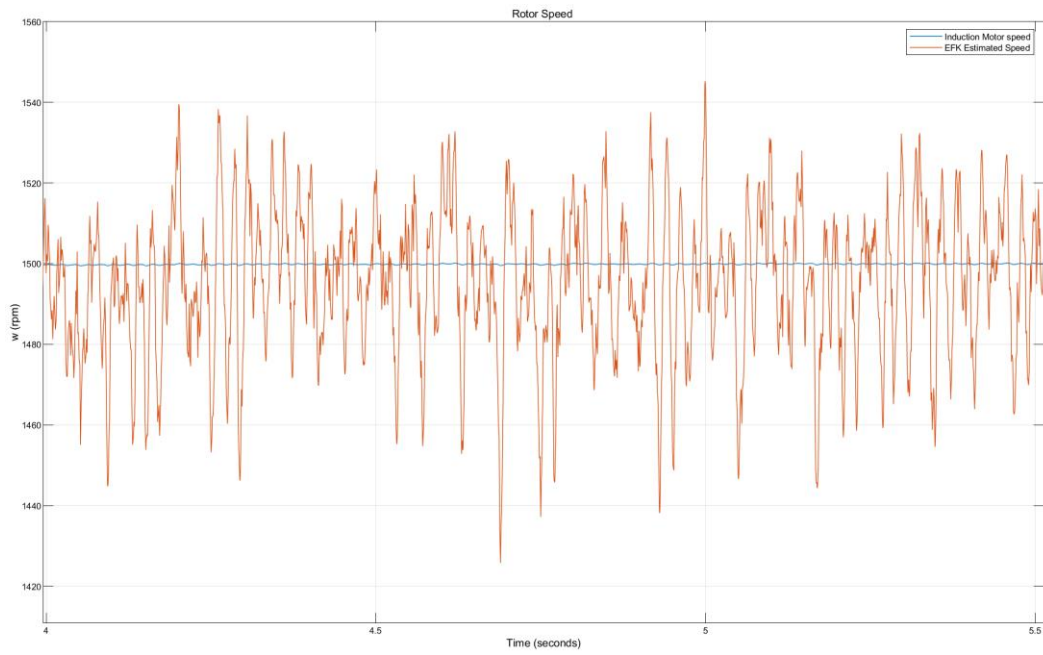


Figure 3.11: Detailed view of the speed comparison in steady state for Figure 3.10

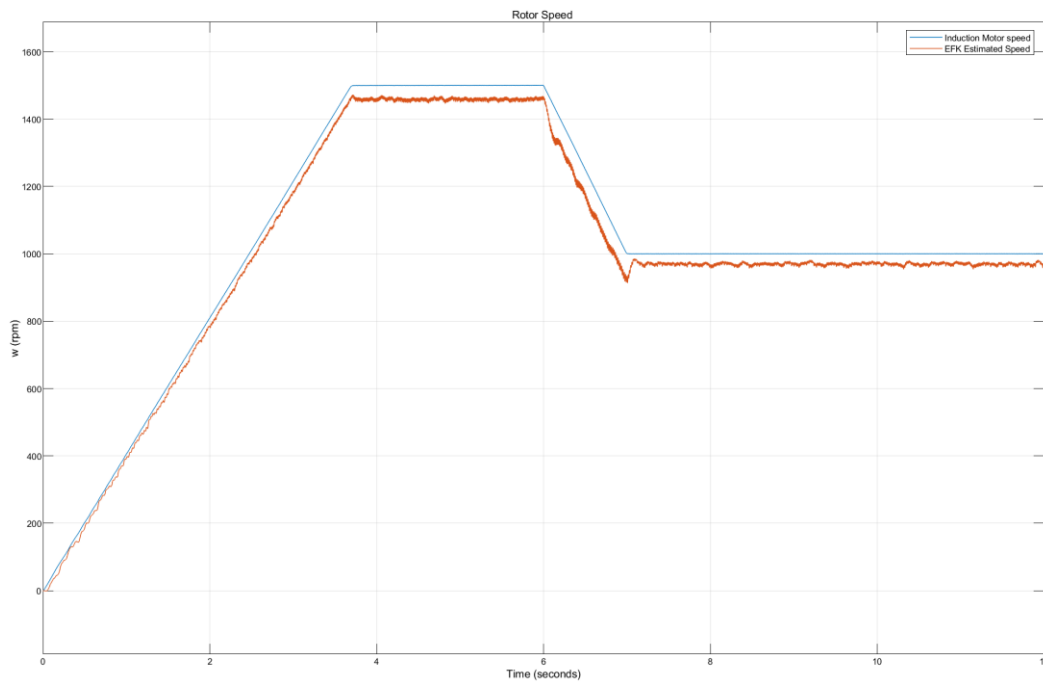


Figure 3.12: Simulation result comparison between Measured IM speed and EKF estimated speed for  $150\mu\text{s}$  sampling time with noise.

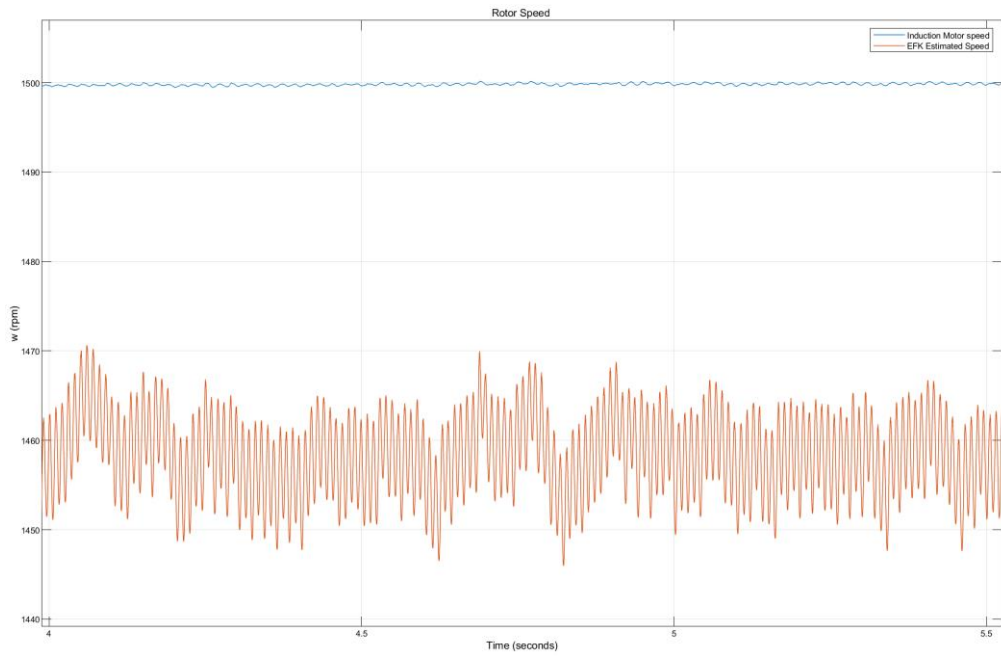


Figure 3.13: Detailed view of the speed comparison in steady state for Figure 3.12

The two different cases of differing sampling time are shown in the above 4 sets of figures. From the above results, we can see that the lower sampling time makes the estimations more accurate and as the sampling time increases the offset is more.

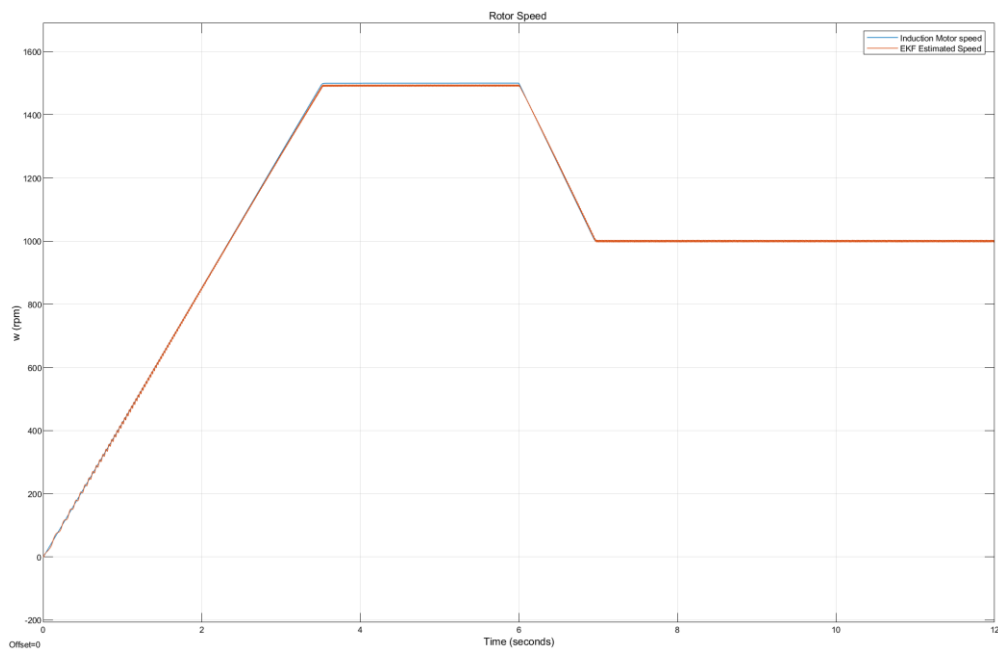


Figure 3.14: Simulation results without any noise and added offsets in the Measured and Estimated speeds.

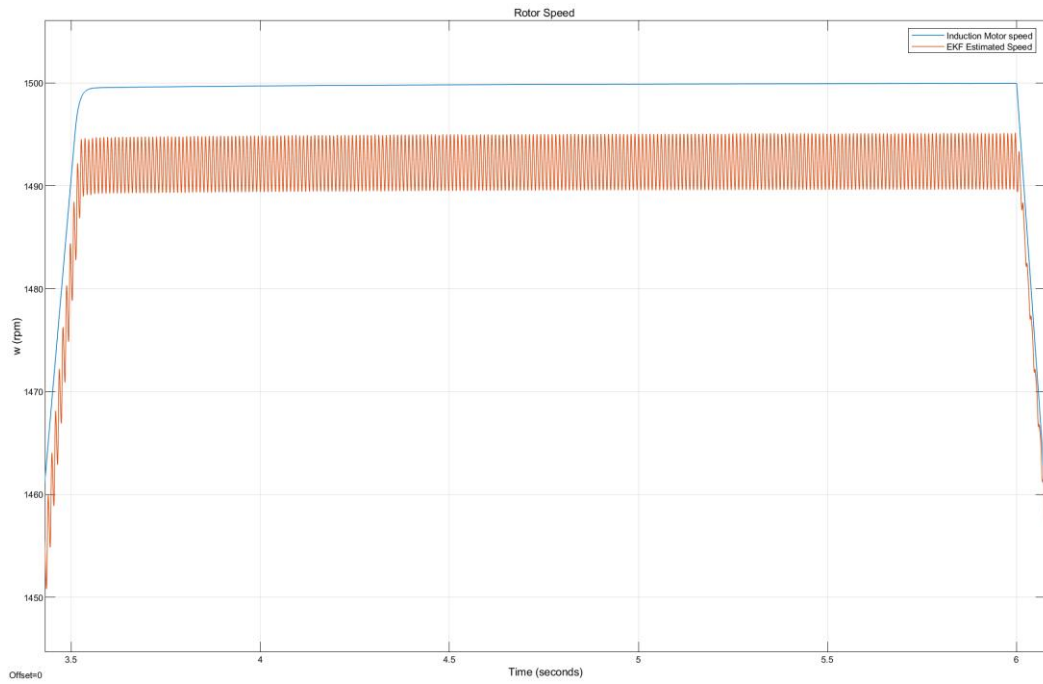


Figure 3.15: Detailed view of the speed comparison in steady state for Figure 3.14

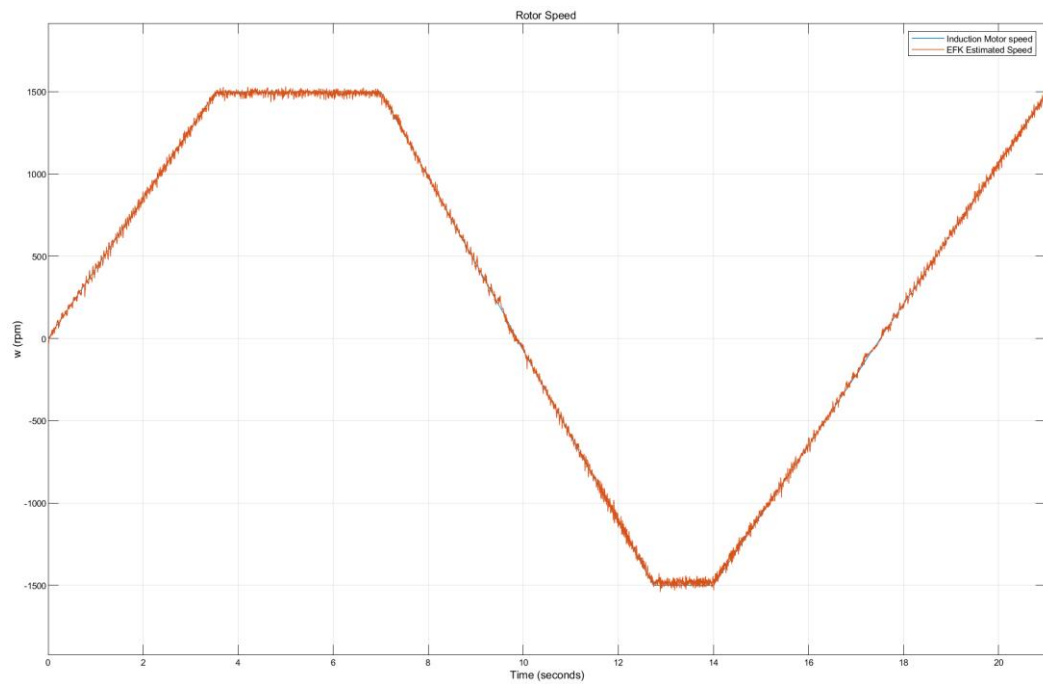
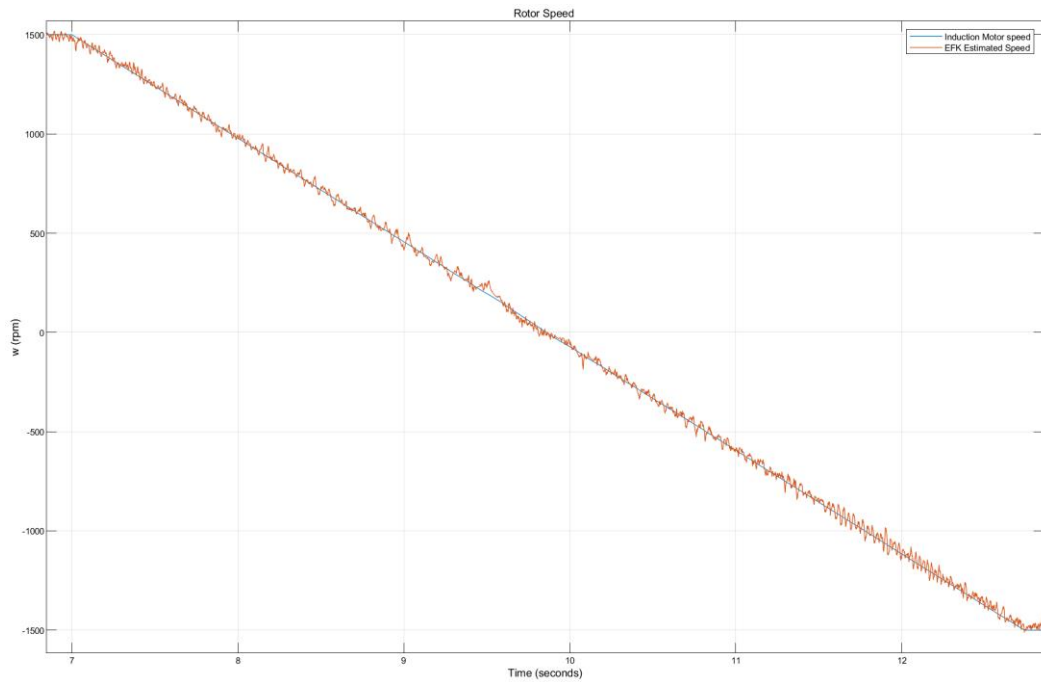


Figure 3.16: Simulation result comparison between Measured IM speed and EKF estimated speed for  $20\mu\text{s}$  sampling time and observing the state of speed reversal with noise.





*Figure 3.17: Detailed view of Figure 3.16 in the speed reversal region*

In the above figures, we can see that the filter algorithm works reliably under the condition of speed reversal as well, as the reference is changed from 1500 rpm to -1500 rpm and back to 1500 rpm.

### **3.4 Concluding the Simulation Results**

From the above figures and results, we can validate the estimation made by the EKF algorithm that has been developed. Presented Figures show the transients, steady states and the speed reversal conditions of the motor. From, the two different cases of differing sampling time that are shown in above figures, we can conclude that the lower sampling time makes the estimations more accurate and as the sampling time increases the offset is more. And the results without noise are very accurate with less offsets, while even with noises the model works reliably. These results give validation to proceed with the simulation to laboratory hardware assembling and implement the filter on a real drive with induction motor. On the next chapter, we will evaluate the workplace of the laboratory where the filter model will be implemented.

---

## Chapter 4

### Description of the Workplace and Hardware Assembled

In previous chapter, we discussed the simulation results and their validity to proceed with the hardware assembling and laboratory implementation of the speed estimation model with EKF. The real drive with induction motor was assembled in the laboratory H26, Department of Electric Drives and Traction, Faculty of Electrical Engineering.

#### 4.1 The Circuit Diagram

The circuit diagram of the assembled circuit is given below in Fig 4.1:

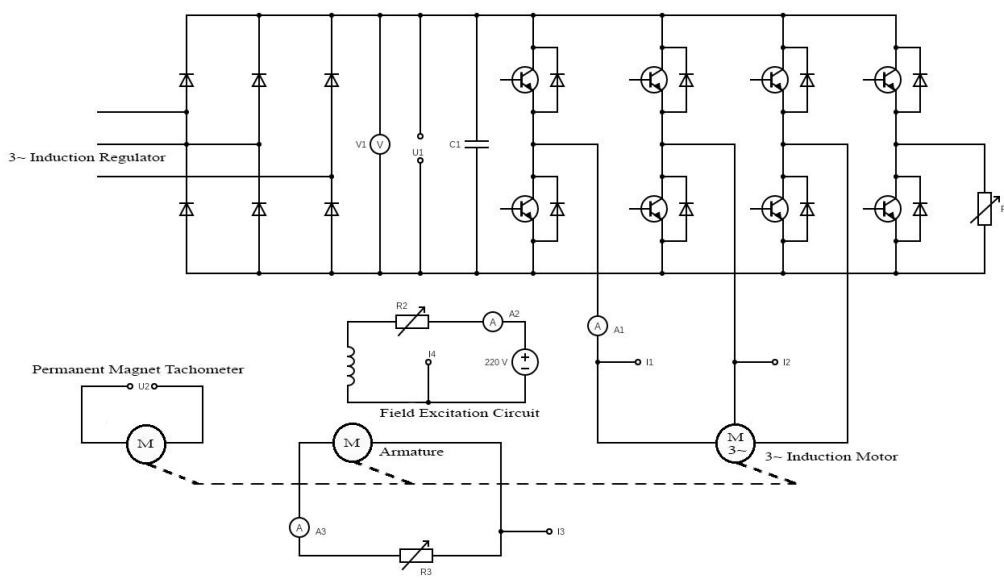


Figure 4.1: Circuit schematic of the assembled circuit

#### 4.2 List of Hardware assembled

The list of hardware assembled for the realization of the schematic is as follows:

1. Rectifier: M Diode Rectifier  
Rated Current: 63 A  
Rated Voltage: 600 V

---

2. Current and Voltage Measurement interface for the DS1103:

Rated Current: 200A

Rated Voltage: 800V

In every LEM current sensor, there was five turns of the phase wire in order to increase the measurement accuracy, so the maximum current for each coil was 40A. Since the induction motor rated current is 2A only, more turns could have been present in order to increase the accuracy more. But because of the space limitation we could not accommodate more coil turns to increase the accuracy of the sensor.

3. IGBT:

6 CM100DY-24NF IGBT [11] by Mitsubishi Electric used for motor control, with 2 more used as a safety layers in case of overvoltage , with a break resistor R1 rated at 420Ω.

4. DC-Link Capacitors:

Rated Voltage: 450 V

Rated Capacitance: 4700 μF

Two capacitors of the above rated parameters each, connected in series to make capacitor bank for the DC-link.

5. Induction Motor:

Y-connected

Rated Voltage: 380 V

Rated Current: 2 A

Rated Power: 750 W

Nominal speed: 1380 rpm

Power Factor (cosφ): 0.79

Frequency: 50 Hz

6. DC Motor:

Rated Power: 1.2 kW

Armature:

Rated Voltage: 400 V

Rated Current: 3.8 A

---

Field Excitation Circuit:

Rated Voltage: 220 V

Rated Current: 0.6 A

Nominal Speed: 1650 rpm

7. Permanent Magnet Tachometer:

Tachometer aligned to the same shaft as the DC motor and Induction motor. The tachometer is calibrated at 80V/1000 rpm

8. Resistors:

For overvoltage protection (R1): 1.2 A 420  $\Omega$

For DC motor Field excitation (R2): 4 A 39  $\Omega$

For DC Motor Armature Winding (R3): 0.63 A 200  $\Omega$

(3 resistors used in series) 1.6 A 250  $\Omega$

2.5A 105  $\Omega$

9. DS1103 PPC Controller Board [12]:

The dSPACE board is used as a microcontroller along with its controller UI desk. In the above circuit the measurements from the points U1, U2, I1, I2, I3 and I4 are taken to process and compute the required measurement quantities. U1 was used for the dc-link voltage for the inverter calculations, U2 was used to get the measured speed of the motor, I1 and I2 for the stator current measurements and I3 and I4 for the load measurements.

10. Voltmeter:

One Voltmeter rated at 600V is used to check the DC-link voltage.

11. Ammeter:

Three Ammeters are used at: the Excitation winding of the DC motor, Armature of the motor DC motor, and the input to one of the windings of the Induction motor. There were used to ensure the currents do not exceed the rated current while changing the load values for the experiment. DC ammeters and AC millimeters were used accordingly in circuits.

---

12. Oscilloscope:

Rohde and Schwarz RTO 1004 Oscilloscope used for visualization of results in the real time interface and collection of data points for further processing.

The measurement data collected were obtained from the Oscilloscope. The Oscilloscope was given inputs from the output of the DAC ports from the DS1103 board. The measurement data were stored in the Oscilloscope memory and collected.

The picture of the assembled hardware is presented below.



*Figure 4.2: Workplace and the assembled hardware*

Besides the hardware, the dSPACE control desk project UI is presented below in Fig 4.3. The Matlab Simulink file was compiled and uploaded into the DS1103 and the control UI was the dSPACE control desk from the laptop.

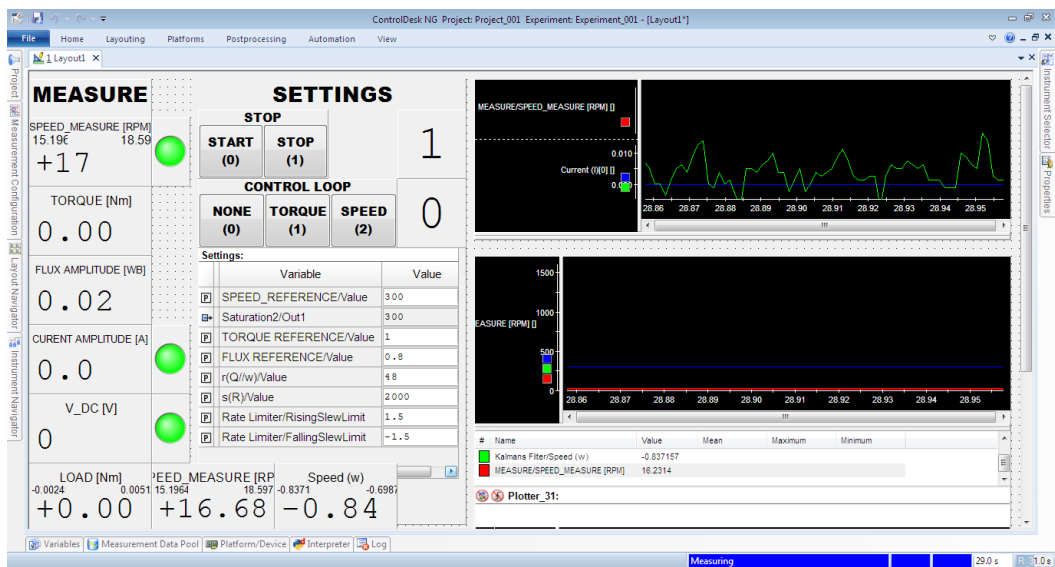


Figure 4.3: dSPACE control desk project UI

---

## Chapter 5

### Experimental Results

After assembling the hardware, we experimented the various cases of the motor operations that included the loaded and unloaded operations, changing the values of filter noise covariance matrices  $Q$  and  $R$  and their effects on transient and steady-state performances and tuning them based on the desired operation, low speed performance and the performance under varying load.

Regarding the sampling time of the experimentation loops, all the experimentation was done with a sampling time of  $150\mu\text{s}$ . This is because we could not gain a better sampling time in the experimentation due to the computational limitation of the hardware used (DS1103) and computational requirements of the filter.

#### 5.1 Steady State Operation of the Motor.

##### 5.1.1 Loaded steady state operation of the motor.

We evaluated the operation of the motor under loaded conditions, under varying speeds. The following graphs show the result of the experimentation. The measured and estimated speed are shown in Fig 5.1.

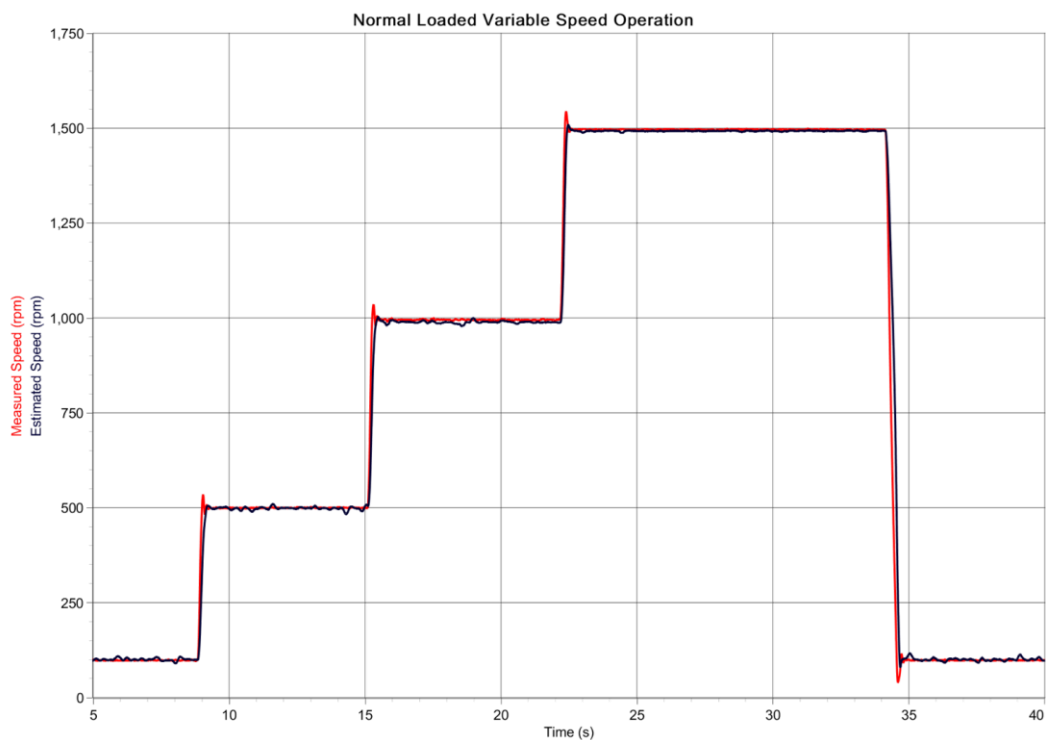


Figure 5.1: Loaded steady state operation of the motor.

The Figure 5.2 shows the detail of the steady state speed of the motor and filter.

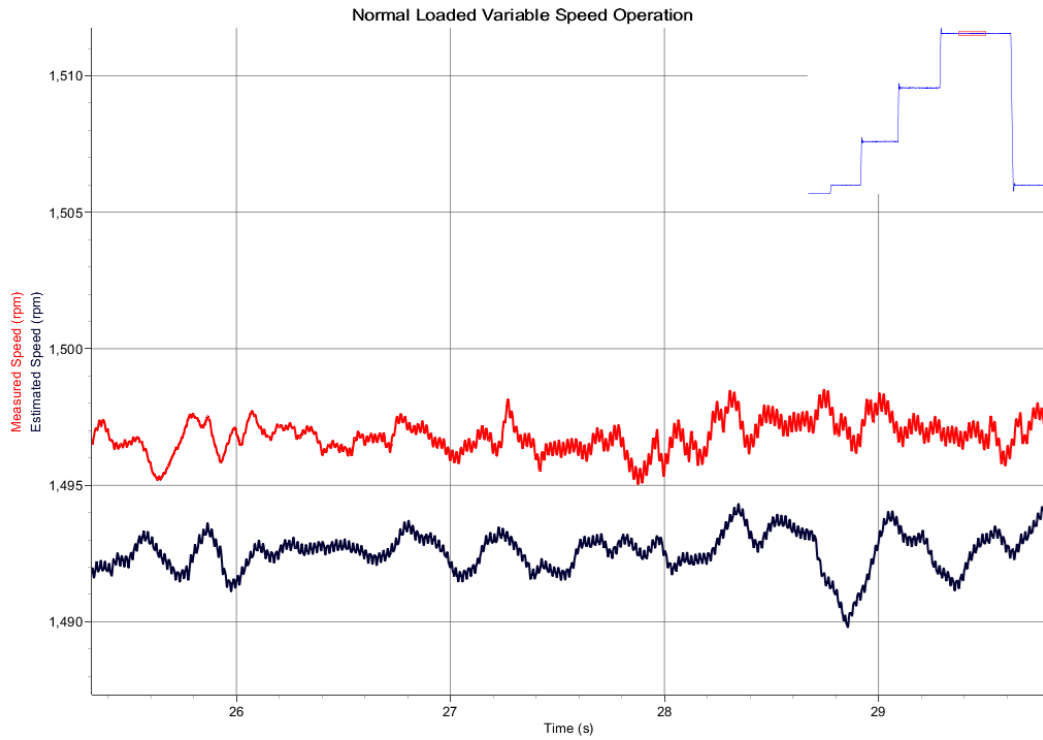


Figure 5.2: Detailed view of Figure 5.1 in the high-speed steady state region.

From the 2 figures, we can see that the normal loaded operation of the motor and its estimated speed from the EKF is not very different. It can be seen that the offset is very low in the loaded condition. The unloaded conditions are evaluated below.

### 5.1.2 Unloaded steady state operation of the motor.

After evaluation of the loaded conditions of the motor we did an experiment run without any load on the motor (minimal load possible), the results of the unloaded experiment is presented below. From the presented results it can be seen that the offset in the unloaded conditions is higher than in the loaded condition.



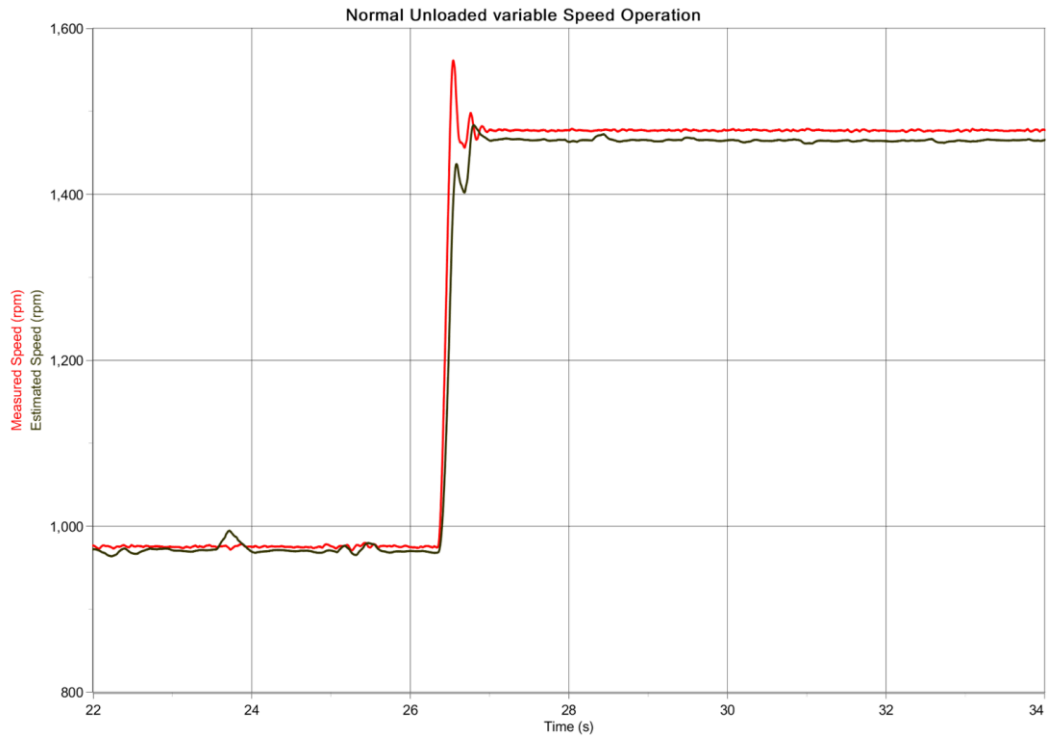


Figure 5.3: Unloaded steady state operation of motor.

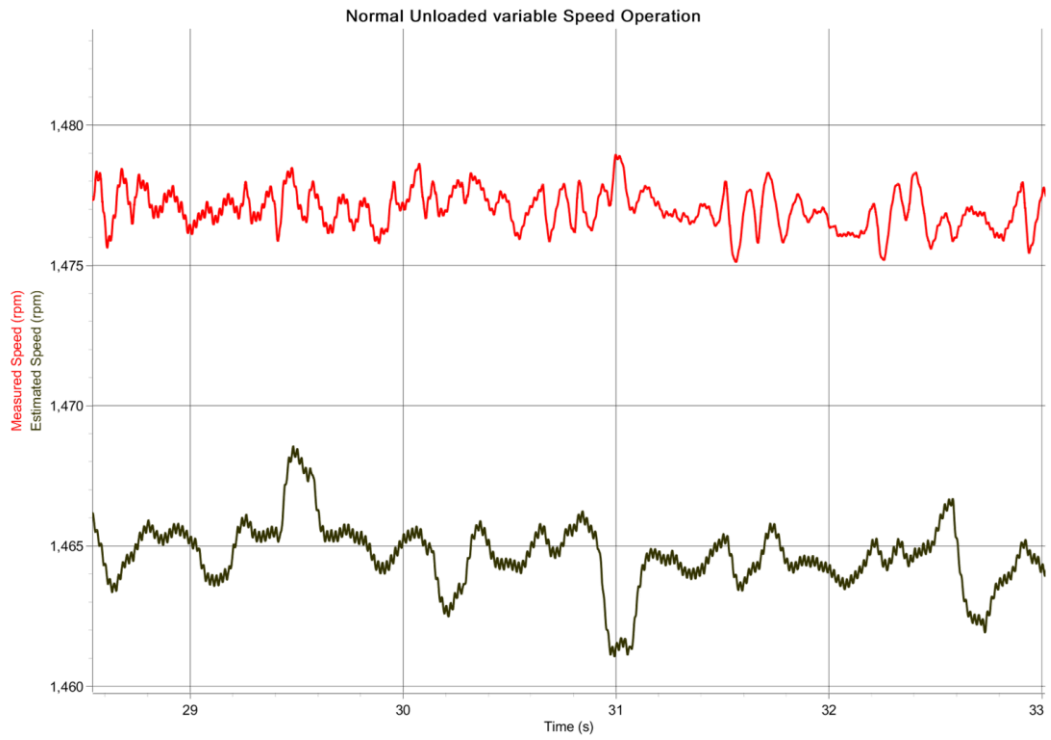


Figure 5.4: Detailed view of Figure 5.3 in the high-speed steady state region.

---

### 5.1.3 Comparison of loaded and unloaded operation mode

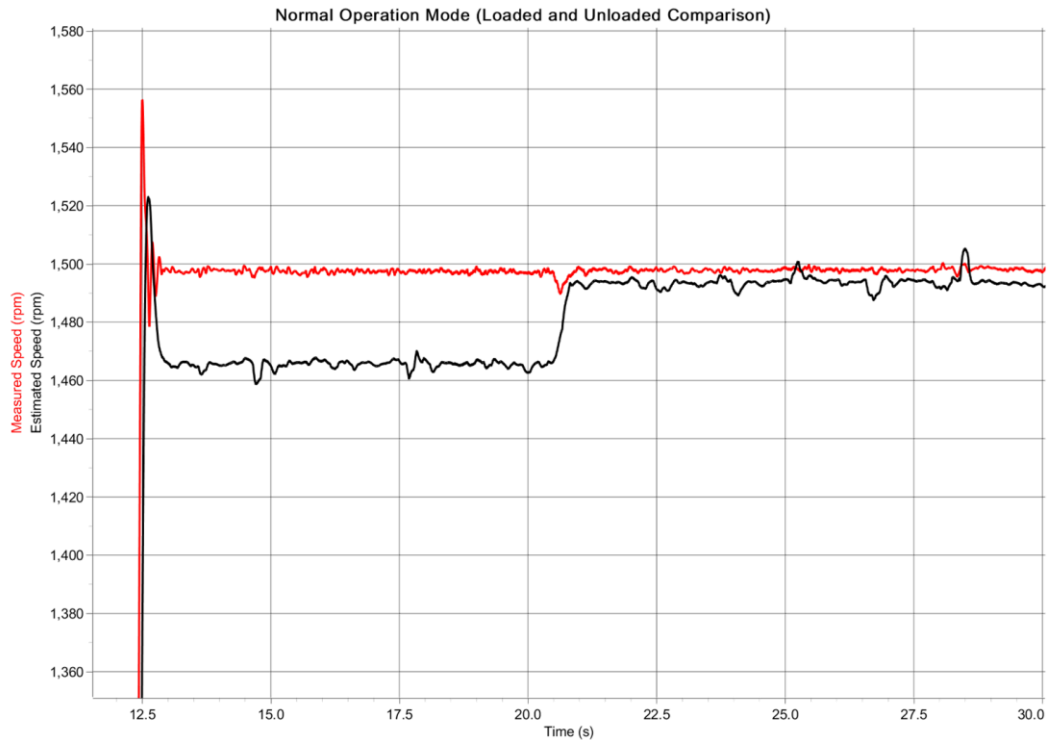


Figure 5.5: Comparison of loaded and unloaded operations mode in steady state

In Fig 5.5, we can see the comparative results of the operation of the motor initially under unloaded condition. When running the motor around 1500 rpm, we can see that the offset is significant in the unloaded case. At around 21s, the load is switched on. The following section in the oscillograms after 21s shows the changes in the estimated speed and its reduced offset. The changes in the loaded and unloaded conditions are due to the effectiveness of the measurement of current from the current sensors. With higher load, the current is more precisely measured and the estimation is better computed using the measured currents. This is evident from the above figures.

## 5.2 Tuning of covariance noise matrices Q and R

Earlier we discussed the effect of changing the covariance noise matrices Q and R on the effect of the estimation during tuning the EKF. In the following section, we discuss the experimental results from the collected data about the effect of varying Q matrix while keeping R constant and vice versa. From this measurement and discussion of the results, we can tune the filter for transient or steady state performance.

---

### 5.2.1 Keeping R constant and varying Q in steady state

Like we stated in chapter 3 we are only tuning for the  $q_{55}$  in matrix Q when we are tuning for matrix Q.

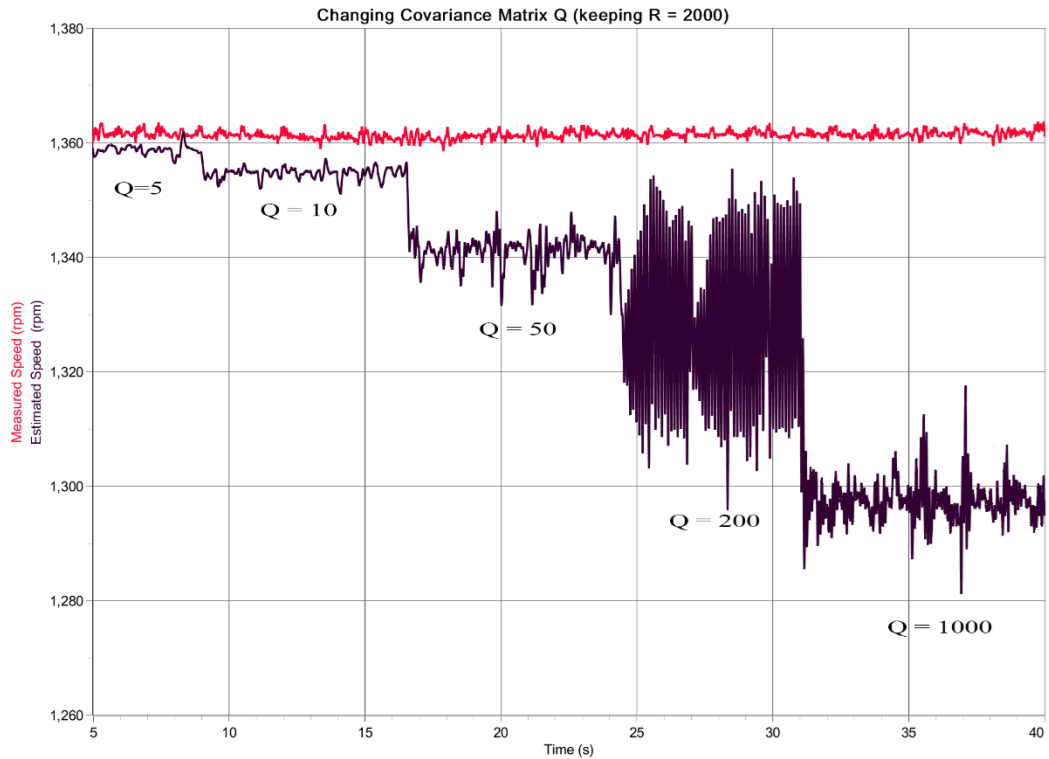


Figure 5.6: Varying Matrix Q while keeping R constant at 2000 in steady state.

From the figure, we can see that the higher the value of matrix Q, the higher the offset from the measured value in the mean position. We can conclude from this that the matrix Q has to be stabilized to lower values for the more stable and reliable estimation.

### 5.2.2 Keeping Q constant and varying R

For matrix R the diagonal elements  $r_{11} = r_{22}$ . Like in the case of tuning for matrix Q, for matrix R also we changed the value of R and while keeping Q constant at 10.

From figure 5.7 below we can see that, higher values of R causes lower offset and as the value of R decreases the offset increases significantly.

From the tuning of Q and R in steady state regions we can say that higher values of R and lower values of Q are more desired for more stable and reliable estimation from the EKF.

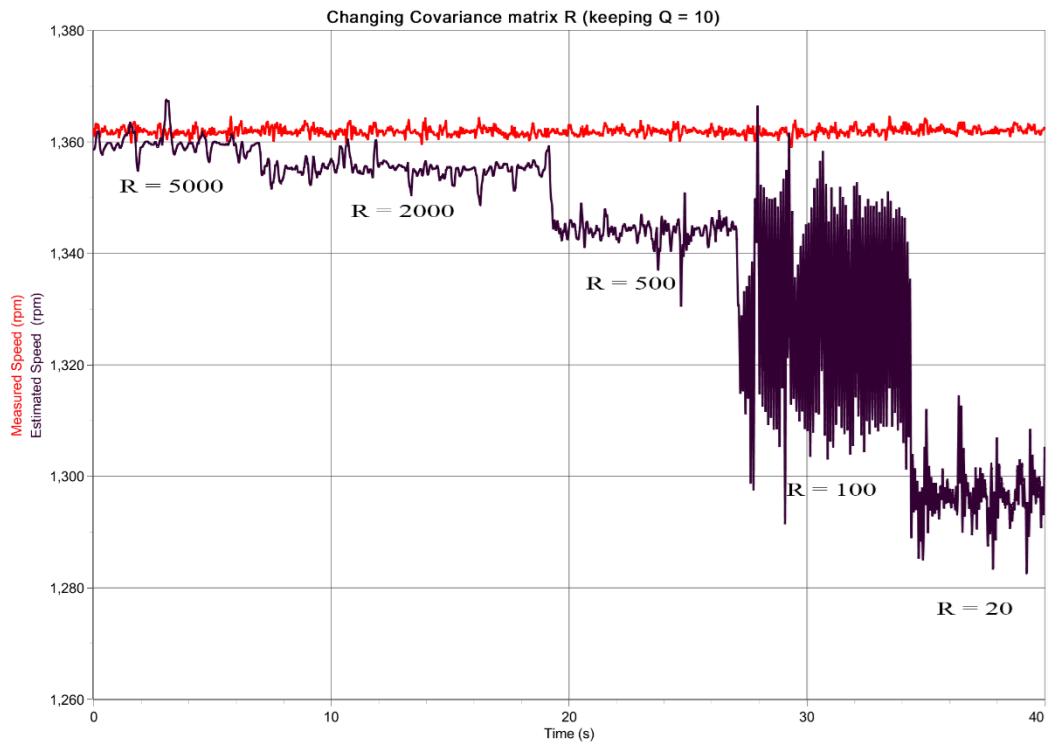


Figure 5.7: Varying Matrix  $R$  while keeping  $Q$  constant at 10.

### 5.2.3 Varying $Q$ while keeping $R$ constant at 2000 in transients.

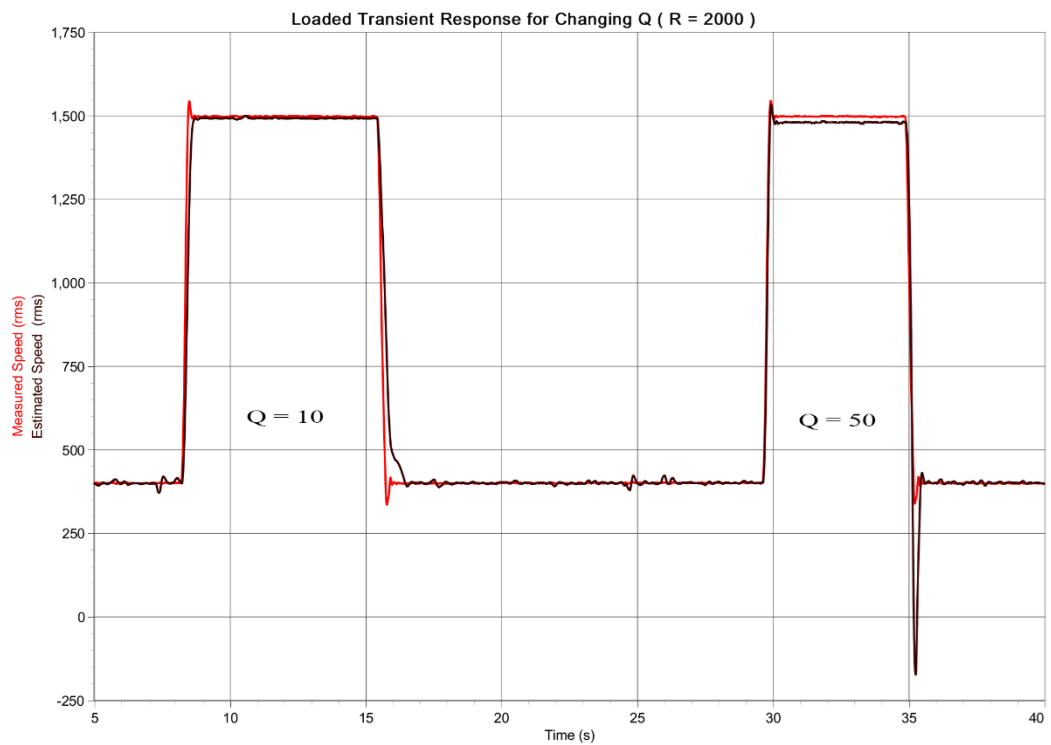


Figure 5.8: Varying Matrix  $Q$  while keeping  $R$  constant at 2000, for transient response.

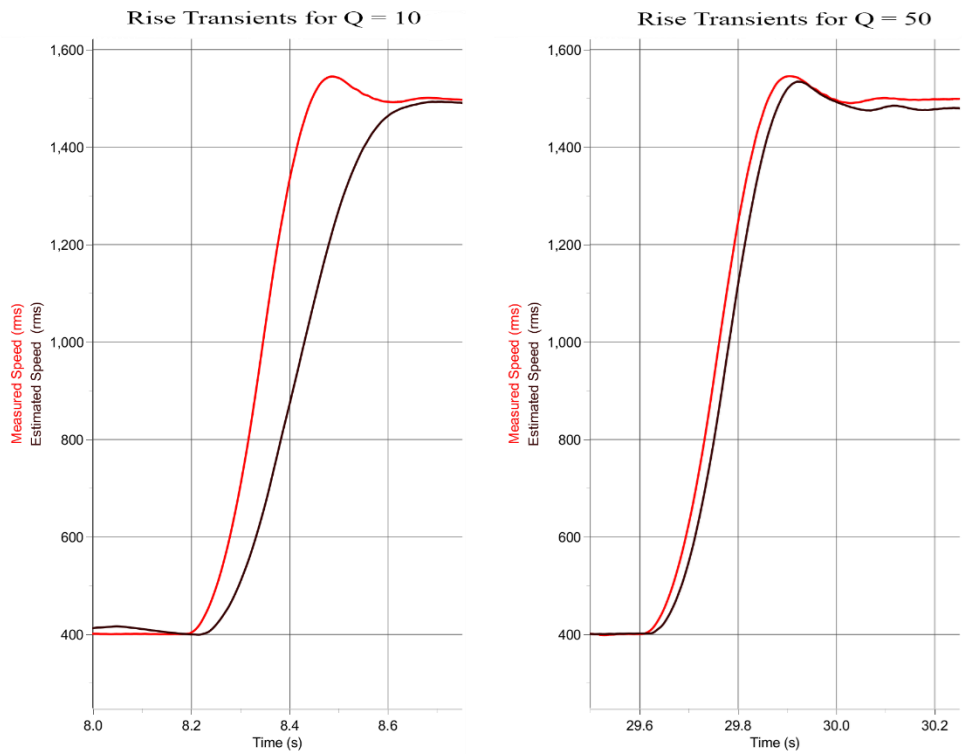


Figure 5.9 Comparison of rise time during transients for different  $Q$  values ( $R = 2000$ )

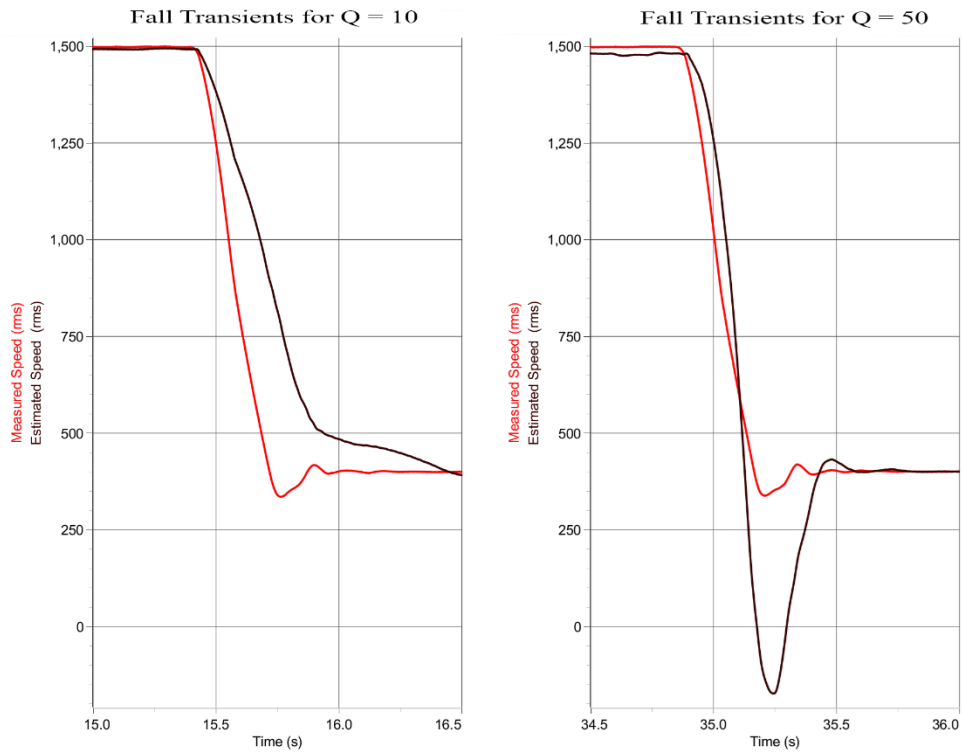


Figure 5.10: Comparison of fall time during transients for different  $Q$  values ( $R = 2000$ )

In figure 5.8 we can see the transient responses for 2 different values of  $Q$ . Figure 5.9 shows the comparison of rising transient characteristics. From the figure, we can see that the rise time for higher  $Q$  value is faster and the estimation is more accurate than for the lower  $Q$  value. In figure 5.10, we can see the fall transient characteristics. Here in the case of higher  $Q$  value, the transient has better estimation in the initial stage but as the final value is reached the estimation has an overshoot peak, which is damped very quickly though. However, in the case of the lower  $Q$  value, the fall time is much higher and the deviation is higher in estimation as well.

From the above experimentation, we can say that the lower  $Q$  values are preferred in stable states and moderate  $Q$  values are preferred for the faster transients. For a mixed operation, the balance between lower offset and faster transient is chosen as per the necessities. Because of this reasons for all the experimentation, for steady state  $Q = 10$  and  $R = 2000$  is taken, and for the transients,  $Q=50$  and  $R = 2000$  is taken.

### 5.3 Operations in Speed Reversal Mode with changing slew rates.

During experimentation, we evaluated the speed reversal condition of the motor. The reversal was done for varying slew rates and the effect of the slew rates was observed. Three different slew rates of 0.05 and 1.5 were observed for loaded condition and the slew rate of 1.5 was observed for the unloaded condition.

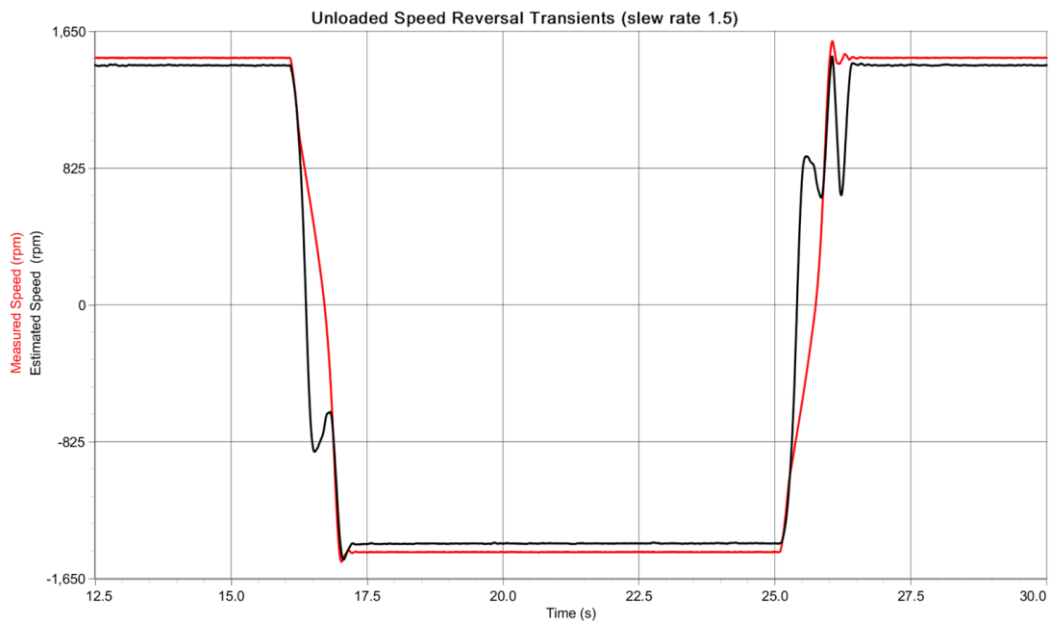


Figure 5.11: Unloaded Speed Reversal Transients with slew rate of 1.5

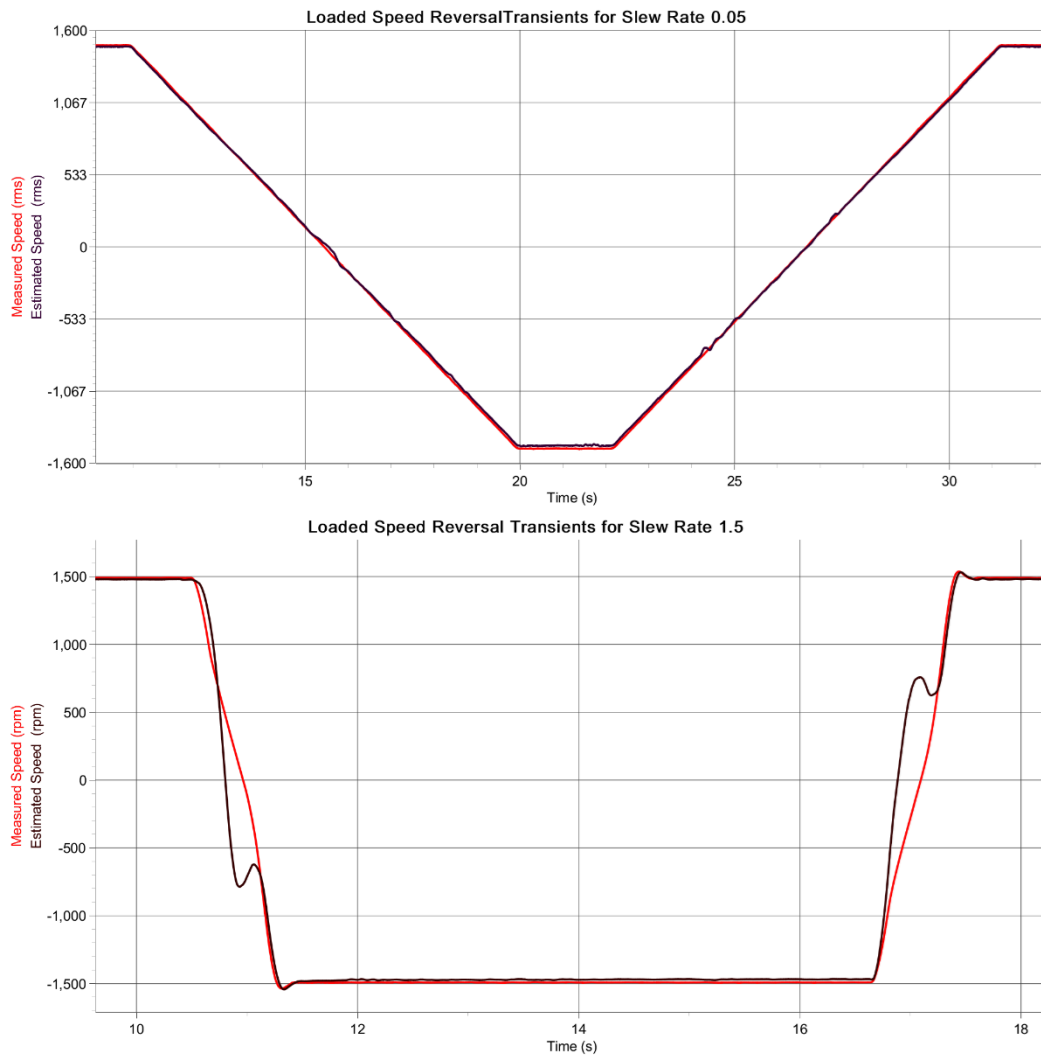


Figure 5.12: Comparison of loaded Speed Reversal Transients with slew rate of 0.05 and 1.5

**Reference:** a slew rate of 0.05 takes 9 seconds to fall or rise 3000rpm, while a slew rate of 1.5 is much quicker to fall or rise with only about 0.75s to rise or fall similar range of 3000 rpm. A higher slew rate shows the faster change.

In figure 5.12 we can see that the estimation from EKF looks very approximate with the measured speed under the lower slew rates, while in the faster transients the deviations and midway overshooting is observed. The offset in the steady-state region is also very moderate in loaded conditions as compared to the unloaded conditions too. And for the unloaded condition from figure 5.10 the transients look much more unstable and multiple overshoots are observed midway. For faster transients, the speed reversal at surrounding areas of 0 has higher deviations in the midway regions for both loaded and unloaded conditions. The filter estimation is deviating highly from the actual measured

---

speed in those regions. But for the lower slew rates, the same problem is not observed as seen in the above graphical results.

## 5.4 Low-Speed Performance

The low-speed performance of the filter is presented below. In figure 5.13, we can see that the performance of the filter is less reliable as the speed reaches towards zero crossings for the speed reversal. The deviations are highest around the zero crossings. Filter reliability is greatly reduced in the areas between the ranges of +20 to -20.

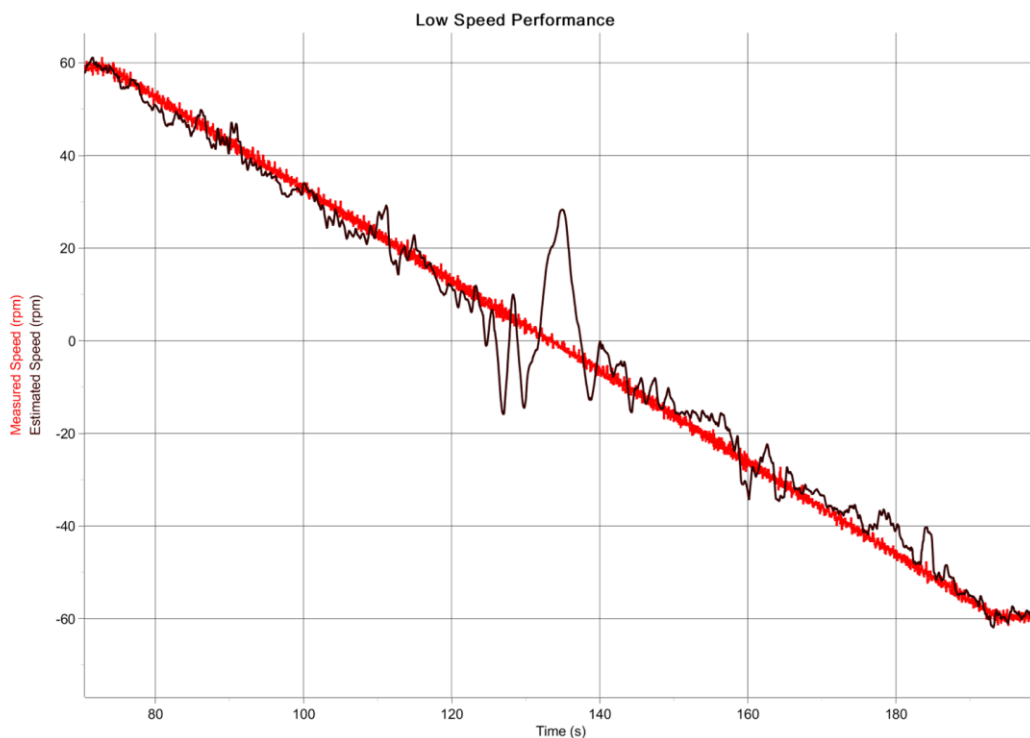


Figure 5.13: Low-Speed performance with zero crossings (60 to -60)

## 5.5 Performance under varying load.

Upon the completion of all the other experimentation, we tested the operation of the motor under varying loads and the change in torque generated by the motor. The relation between torque generated by the motor and the change in the speed of the motor accordingly was observed. The induction motor speed was controlled by the PI controller and the load was adjusted by the variable resistor in the DC motor armature circuit. The



load was started from minimum and set to generate around 4 Nm torque in the peak conditions. The developed graphical results are presented below.

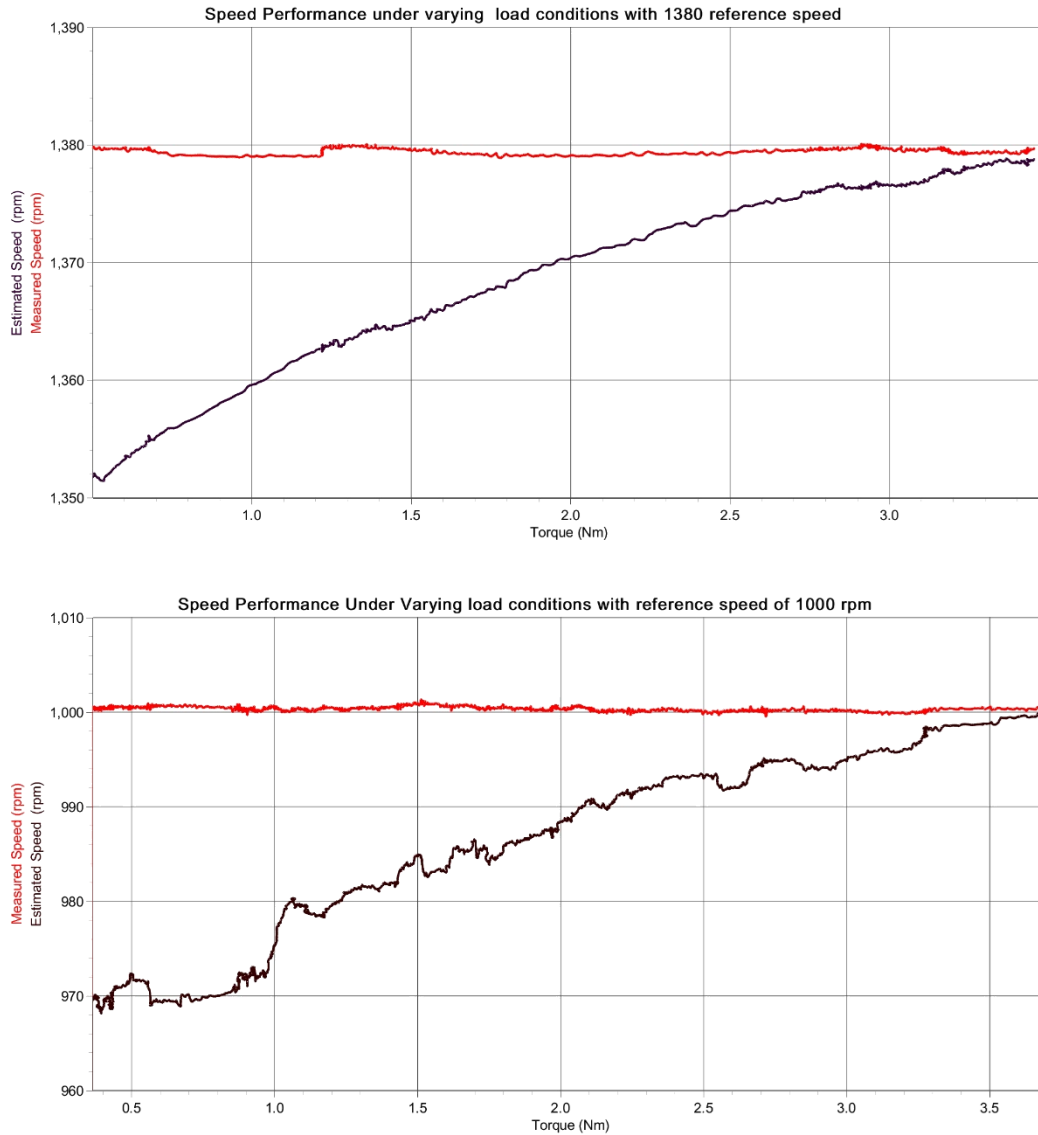


Figure 5.14: Measured and Estimated speed under varying loads with various speed references

From the above figure, we can see that the filter reliability is low when the load in the motor is very low as in the unloaded operations. But as the load increases the filter reliability increases and the offset is reduced. Near the regions of the optimal load, the estimated speed from the filter is as close as the real measured speed.

---

## *Chapter 6*

### **Conclusion**

Motor control has been an essential part of the industrial sector. With the automated controls, we are moving farther and distant from the manual controls every other day. The reliance on sensors has been decreasing and the automation towards sensorless controls has been the new wave of control mechanisms. The elimination of sensors makes the control strategy more economically viable. With the increasing computational power of smaller ICs, the dependence on the algorithms for estimations of speed with high reliability on the output has been a greater advantage for this control sector. Going with the theories behind one of the estimation algorithms, in this thesis paper we tested one of such algorithms: Extended Kalman Filter. An EKF was designed, developed, and implemented with the hardware realization on a laboratory motor.

The results of the experiment were in accordance with the simulations. The hardware implementation in this project paper gave the idea of the difficulties when moving from simulation model to real hardware. One of such instances was the limitation of the computation power of the signal processor used. While in simulations, the lower sampling times were achieved with lower offsets, in the hardware scenarios, the sampling times were limited to  $150\mu\text{s}$ . This led to the expectation of the offsets in the estimated results from the EKF. While in some fronts the hardware developments with the real-time interface were much easier to control than in simulations, like the tuning of the filter covariance matrices and the assessment of the transient dynamic.

The results in this thesis show the effectiveness of the filter with low error percentages under the right tuning of the filter covariance matrices. The results show that tuning of covariance matrices in the filter plays a big role in the ultimate output of the filter and its accuracy. As discussed prior, based on the suitability of the applications being transient analysis on the motor or the steady-state responses of the motor the tuning should be done accordingly. The results from chapter 5 show the differences in the tuning parameters, and their necessity to be chosen appropriately.

With the right tuning parameters, the filter accuracy can be discussed from the results very clearly. The loaded and unloaded operation of the motor shows the difference in offsets, mainly due to the current sensitivity of the current sensors used. We can state

---

from the loaded conditions that the filter behaves very accurate even under unloaded conditions if more sensitive current measurement devices are taken into consideration. Similar to the loaded and unloaded operations in steady-state conditions at normal speeds, the performed tests show that the filter works properly in speed reversal conditions as well. This is an important aspect in the case of bidirectional motors. The reliability of the filter in both the direction of the rotation axis shows the filter versatility and accuracy.

For the low-speed regions, the reliability of the filter has been worse. There is a room for improvement in the filter algorithm that can access these low-speed estimations with very low-speed dynamics during speed reversals near zero crossings.

Besides the low speed and offset issues, other regions for decreased reliability in the filter could be because of the system description not being 100% accurately described. The parameters of the motor were measured in certain operation point (loaded motor) and with some uncertainty. Moreover, the changes that occur with the temperature resistances and load magnetization curves of inductance is not taken into consideration. Also the sampling time taken from the computational device is very long. And the measurement of current was in the range of 40A accuracies while the motors nominal current was around 2A. The voltages were calculated from the DC link and transistor combination, so the other nonlinearities in the model due to switching time delays and voltage drops of the inverter are also not considered. In regards to these factors not being in consideration, the estimation can be made better with the inclusion of these factors in future.

Overall the development and performance of the filter from this thesis experimentation and simulation can be said to be accurate small deviations and offsets in nominal steady states, while the room for improvement is always there. The tested results for various operating conditions as discussed above serve as backing data for the effectiveness of the filter developed.

### **Work for Future.**

While the extent of this thesis was limited to the estimation for the speed of the IM without any speed sensors, the work from this experiment can be carried further ahead on the other control experiments. The estimated speed can be fed back as a closed loop control for sensorless vector control of the IM. This regime of control is the new control

---

strategy that is more economic with the employment of fewer sensors and is also economically more suitable.

Further work can be done as discussed above on the better representation of the model considering all the other factors stated above. Besides that the computational requirements can also be reduced for faster sampling times with code optimization.

---

## Chapter 7

### References

- [1] F. Wang, Z. Zhang, X. Mei, J. Rodríguez, and R. Kennel, "Advanced control strategies of induction machine: Field oriented control, direct torque control and model predictive control," *Energies*, vol. 11, no. 1, 2018.
- [2] R. Gunabalan, V. Subbiah, and B. Reddy, "Sensorless control of induction motor with extended Kalman filter on TMS320F2812 processor," *Measurement*, vol. 2, no. 5, pp. 14–19, 2009.
- [3] T. RAMESH, A. K. PANDA, S. . KUMAR, and S. BONALA, "Sensorless control of induction motor drives," *Proc. IEEE*, vol. 90, no. 8, pp. 1359–1394, 2002.
- [4] G. Welch, G. Bishop, "An Introduction to the Kalman Filter" , TR 95-041, Department of Computer Science, University of North Carolina at Chapel Hill, Chapel Hill-, NC-27599-3175, 24th July, 2006
- [5] F. Orderud, "Comparison of kalman filter estimation approaches for state space models with nonlinear measurements," ... *Scand. Conf. Simul. ...*, vol. 194, no. 7491, pp. 157–162, 2005.
- [6] M. Madhumita, "Study of Kalman, Extended Kalman and Unscented Kalman Filter (an approach to design a power system harmonic estimator)," 2010.
- [7] Y. Kim and H. Bang, "Introduction to Kalman Filter and Its Applications," *Introd. Implementations Kalman Filter*, no. September, 2018.
- [8] M. I. Ribeiro, "Kalman and Extended Kalman Filters : Concept , Derivation and Properties," *Inst. Syst. Robot. Lisboa Port.*, no. February, p. 42, 2004.
- [9] M.-H. P. Young-Real Kim, Seung-Ki Sul, "Speed Sensorless Vector Control of IM using EKF," vol. 30, no. 5, pp. 1225–1233, 1994.
- [10] P. Karlovsky and J. Lettl, "Induction motor drive direct torque control and predictive torque control comparison based on switching pattern analysis," *Energies*, vol. 11, no. 7, 2018.
- [11] Mitsubishi Electric, "CM100DY-24F", pp. 1–5, 2009.
- [12] dSPACE, "DS1103 PPC Controller Board", pp. 1-8, 2008

---

## Appendix

### A.1 Parameters of IM

The simulated IM's parameters are illustrated below:

Parameters	Values	Unit
$R_S$	10.79	Ohm
$R_R$	6.674	Ohm
$L_S$	0.68487	H
$L_R$	0.68852	H
$L_M$	0.63866	H
P	2	number

### A.2 Equations of IM

The equations used to build the model of IM in Simulink are illustrated below:

$$\begin{aligned}\vec{v}_S &= R_S * \vec{i}_S + \frac{d\vec{\psi}_S}{dt} \\ 0 &= R_R * \vec{i}_R + \frac{d\vec{\psi}_R}{dt} + \omega_R * \vec{\psi}_R \\ \vec{\psi}_S &= L_S * \vec{i}_S + L_M * \vec{i}_R \\ \vec{\psi}_R &= L_R * \vec{i}_R + L_M * \vec{i}_S \\ T &= \frac{3}{2} * P * (\vec{\psi}_S \times \vec{i}_S)\end{aligned}$$